Synthesis, structure-activity relationships, cocrystallization and cellular characterization of novel smHDAC8 inhibitors for the treatment of schistosomiasis

Ehab Ghazy, Tino Heimburg, Julien Lancelot, Patrik Zeyen, Karin Schmidtkunz, Anne Truhn, Salma Darwish, Conrad V Simoben, Tajith B Shaik, Frank Erdmann, et al.

Synthesis, structure-activity relationships, cocrystallization and cellular characterization of novel smHDAC8 inhibitors for the treatment of Schistosomiasis

Ehab Ghazy[1], Tino Heimburg[1], Julien Lancelot[2], Patrik Zeyen[1], Karin Schmidtkunz[3], Anne Truhn[1], Salma Darwish[1], Conrad V. Simoben[1], Tajith B. Shaik[4], Frank Erdmann[1], Matthias Schmidt[1], Dina Robaa[1], Christophe Romier[4], Manfred Jung[3], Ray Pierce[2], Wolfgang Sippl[1,*]

1 Institute of Pharmacy, Martin-Luther University of Halle-Wittenberg, 06120 Halle/Saale, Germany
2 University of Lille, CNRS, Inserm, CHU Lille, Institut Pasteur de Lille, U1019 - UMR 9017- CIIL - Centre d'Infection et d'Immunité de Lille, F-59000 Lille, France
3 Institute of Pharmaceutical Sciences, University of Freiburg, 79104 Freiburg, Germany
4 Université de Strasbourg, CNRS, INSERM, Institut de Génétique et de Biologie Moléculaire et Cellulaire (IGBMC), Département de Biologie Structurale Intégrative, 67404 Illkirch Cedex, France

Abstract

Schistosomiasis is a major neglected parasitic disease that affects more than 265 million people worldwide and for which the control strategy consists of mass treatment with the only available drug, praziquantel. In this study, we chemically optimized our previously reported benzhydroxamate-based inhibitors of Schistosoma mansoni histone deacetylase 8 (smHDAC8). Crystallographic analysis provided insights into the inhibition mode of smHDAC8 activity by the highly potent inhibitor **5o**. Structure-based optimization of the novel inhibitors was carried out using the available crystal structures as well as docking studies on smHDAC8. The compounds were evaluated in screens for inhibitory activity against schistosome and human HDACs (hHDAC). The in vitro and docking results were used for detailed structure activity relationships. The synthesized compounds were further investigated for their lethality against the schistosome larval stage using a fluorescence-based assay. The most promising inhibitor **5o** showed significant dose-dependent killing of the schistosome larvae and markedly impaired egg laying of adult worm pairs maintained in culture.

1. Introduction

Schistosomiasis is a neglected parasitic disease that affects about 240 million people worldwide and is prevalent in poor tropical and subtropical areas. It is estimated that the disease causes more than 200 thousands deaths each year in sub-Saharan Africa in addition to severe morbidity (anemia, growth retardation) and economic losses due to decreased ability of the infected people to work.[1] The infection is caused by blood flukes from the genus *Schistosoma*, mainly *S. mansoni*, *S. haematobium* and *S. japonicum*. As there is currently no prospect of the development of an effective vaccine, efforts to control Schistosomiasis rely almost exclusively on preventive/curative chemotherapy through mass drug administration of Praziquantel.[2] The WHO reports that more than 66.5 million individuals received Praziquantel in 2015. On one hand, this extensive use of Praziquantel has indeed achieved success given that the number of people requiring treatment decreased from around 258.8 million in 2014 to 218.8 million in 2015.[1] On the other hand, this mass treatment using a single drug raises the concern of the development of drug resistance.[3] In addition, Praziquantel lacks efficacy against immature juveniles which can lead to treatment failure.[3-6] Therefore, it is imperative to develop new therapeutic agents and identify novel druggable targets as well as lead compounds to ensure the future of schistosomiasis therapy.

Research on schistosomiasis has recently identified several promising chemical scaffolds that could provide novel therapies.[6] Among these, epigenetic modulators have received great interest. The complex lifecycle of schistosomes, characterized by several morphologically distinct forms, among which the juvenile and adult worms are the infective stages in humans, together with intensive metabolic and reproductive activity, imply a tight control of gene expression to control these changes.[7, 8] Epigenetic modulators of gene expression acting on histones are key to this regulation and are therefore potential drug targets. In this regard, the repurposing of already approved and well-established anticancer drugs targeting histone modifying agents for antischistosomal therapy seems very attractive.[8-10] One of the most investigated posttranslational modification is histone acetylation, where writers, readers and erasers work in concert to control the acetylation state of histone and consequently the activation level of different genes. Of particular importance are the erasers, histone deacetylases (HDACs), as they were found to be deregulated in different human diseases, and inhibitors of human HDACs are either already approved or in preclinical and clinical trials as anticancer therapeutic agents.[11-13] HDAC inhibitors could be utilized as potential antischistosomal agents, as well as against other parasitic diseases.[14, 15]

Histone deacetylases are a group of enzymes that remove the acyl group from lysine residues of histones and some non-histone proteins. In the human, classical HDACs (class I, II and IV) depend on zinc chelation for their catalytic activity, while sirtuins (class III) utilize nicotinamide adenine dinucleotide (NAD^+) for their action.[16, 17] In schistosomes, several orthologues of the human enzymes have been characterized belonging to class I (smHDAC 1, 3 and 8), class II (three HDACs, one related to human HDAC6 and two related to the human clade composed of HDACs 4, 5, 7 and 9) and class III (sirtuins 1, 2, 5, 6 and 7).[18, 19] While class I classical HDACs have received the most interest, several studies also clarified some physiological roles of

schistosomal sirtuins, provided proofs of evidence of the significance of their inhibition, and have recently reported low micromolar inhibitors.[19-21] It was previously reported that the HDAC inhibitor Trichostatin A (TSA) induces hyperacetylation of schistosomal proteins and dose dependent mortality of both schistosomula and adult worms [22] in addition to blocking the transformation from the miracidia into the sporocyst. [23] Class I smHDACs are expressed in all life cycles of the parasite, with the smHDAC8 isoform being the most abundant, whereas its human counterpart (hHDAC8) shows usually a lower level of expression in human cells compared to HDAC,1 and 3. This suggests that this isoform has a specific function for the parasite and could therefore be the perfect target for novel antischistosomal therapy.[8, 24] Indeed, RNA mediated down-regulation of smHDAC8 decreased the ability of schistosomula to survive and mature in infected mice and many selective smHDAC8 inhibitors **(Figure 1)** were reported showing in vitro inhibition of enzymatic activity accompanied by phenotypic effects such as impaired viability of different life stages of the parasite, decreased egg production and morphological alterations in the adult worms.[25-29].

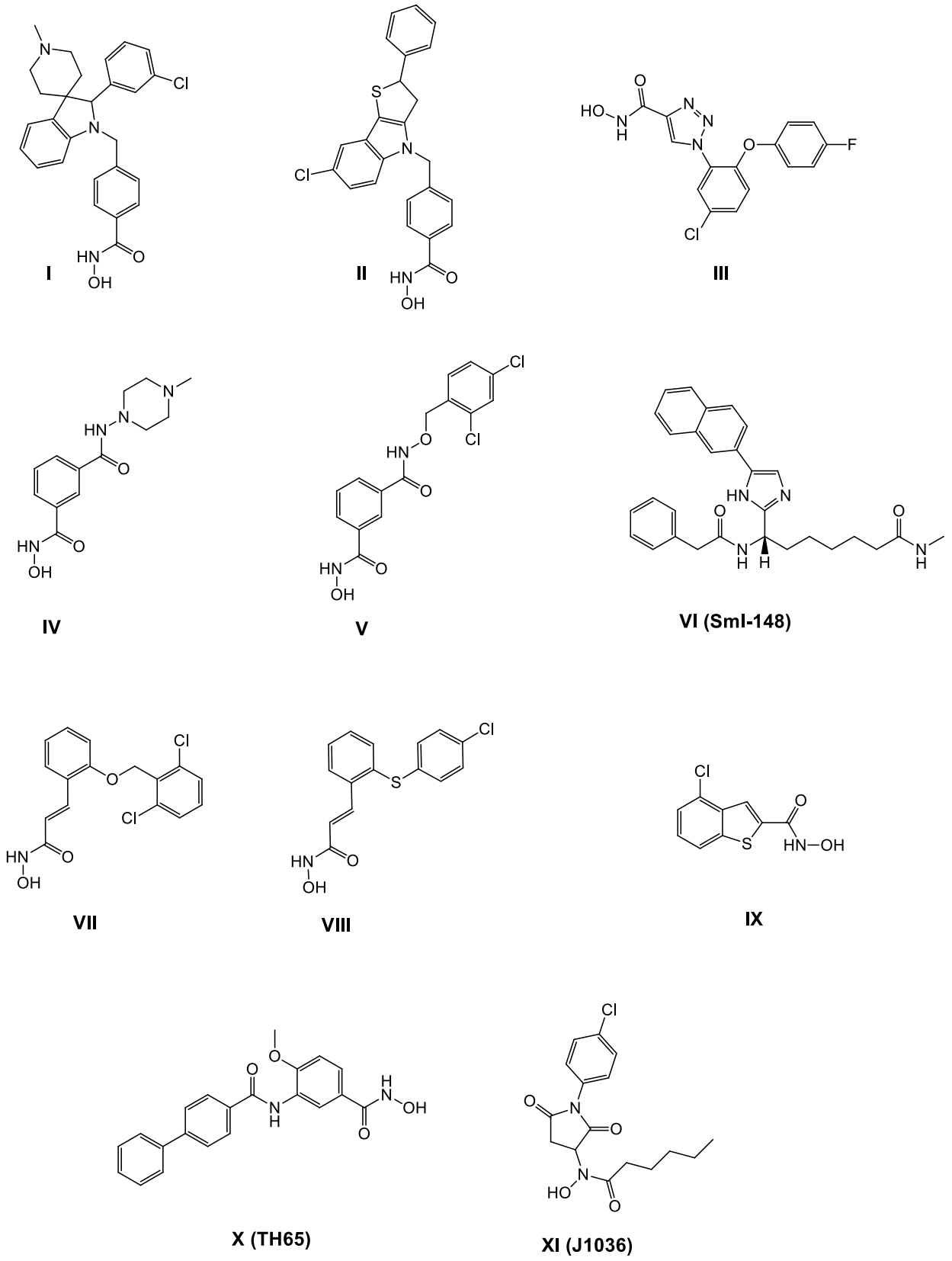

Figure 1: Chemical structures of some previously reported smHDAC8 inhibitors

We have carried out several virtual screens for smHDAC8 inhibitors [30, 31] and identified various hits that were further confirmed through *in vitro* testing. We were able to obtain several crystal structures for some of the hits that interestingly showed different conformations of the binding pocket.[32] Based on the crystal structure of **IX** (J1075**)**, we recently reported an optimized series of cinnamoyl hydroxamic acid derivatives **(Figure 1)** having nanomolar activity against smHDAC8 and also showing a dose dependent mortality on the schistosomula and impaired egg laying of adult worms.[33] Moreover, we previously utilized the crystal structure of **XI** (J1036**)** to guide our structure-based optimization of novel benzhydroxamic acids as nanomolar smHDAC8 inhibitors. The most promising compound obtained was **X** (TH65, **Figure 1)** showing nanomolar inhibition against smHDAC8 (IC_{50} 293 ± 35 nM) as well as dose dependent killing of the parasite larvae (EC_{50} 16.1 μM). It also induced separation of the adult male and female worm pairs with a corresponding reduction in egg laying.[34] The solved crystal structure of smHDAC8 with different selective HDAC8 inhibitors including TH65 allowed the identification of key active site structural and functional determinants important for potent inhibitors.[35]

In the present work we wanted to further explore the SAR of benzhydroxamates as smHDAC8 inhibitors as well as to develop more potent compounds against the parasite. Therefore, we started from the most promising inhibitor, TH65**,** and used structure-based design strategies in combination with synthesis and *in vitro* testing to develop further inhibitor series. We determined the *in vitro* activity of the synthesized compounds against the recombinant parasitic and human enzymes as well as on parasites maintained in culture. Finally, we solved the crystal structures of one highly potent compound in complex with smHDAC8.

2. Results and discussion

Our previous studies have shown that the capping group of the L-shaped *m*-substituted benzhydroxamates occupy the so-called HDAC8-specific pocket; a hydrophobic pocket located between the L6 loop, the L1 loop and Tyr341 of smHDAC8.[34, 35] Since this pocket is not present in the other HDAC isoforms, it can be effectively explored to develop potent and selective HDAC8 inhibitors.

As aforementioned, our lead compound TH65, which bears a biphenyl capping group, was found to show high inhibitory activity against smHDAC8. Structural data revealed that this extended capping group can be well accommodated in the hydrophobic HDAC8-specific pocket, displaying more extensive hydrophobic contacts with Pro291 in addition to the commonly observed pi-pi stacking interactions with Tyr341.[35] This indicated that further exploration of the hydrophobic HDAC8-specific side pocket by bulky capping group is a promising strategy to achieve novel smHDAC8 inhibitors with improved inhibitory activity and enhanced selectivity over human HDAC isoforms (**Figure 2**).

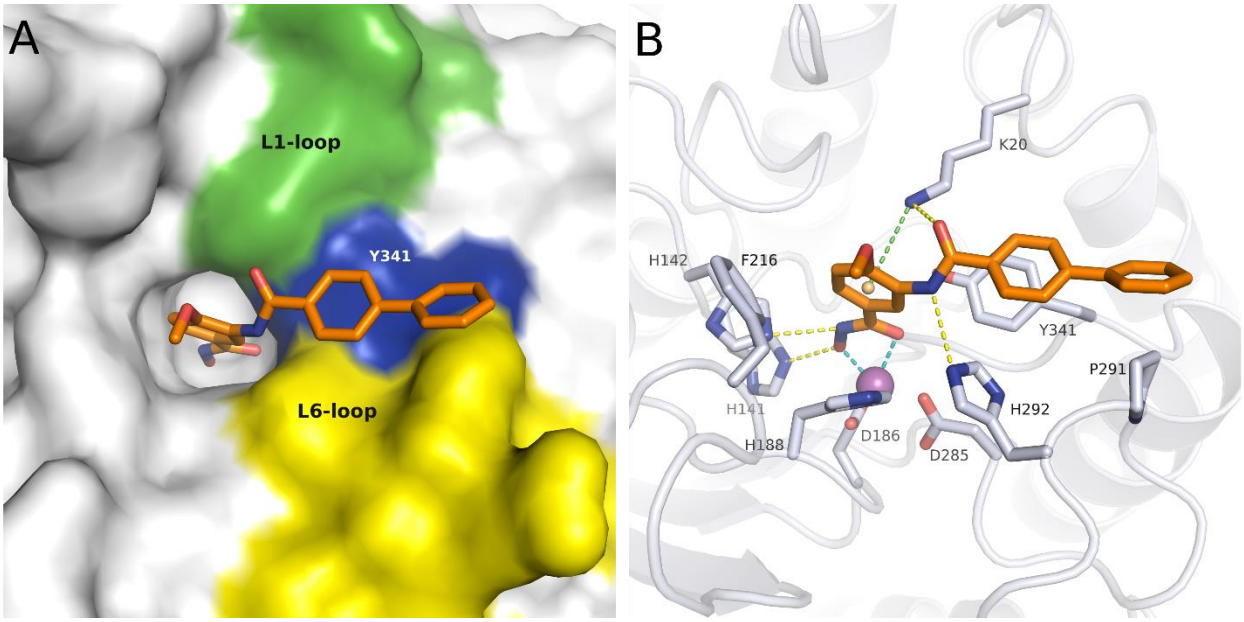

Figure 2: Crystal structure of smHDAC8 in complex with TH65 (PDB ID 6HTH). **A**) Surface depiction of smHDAC8 binding side. The capping group of TH65 (orange sticks) occupies the HDAC8-specific pocket formed between L1 (green), L6 (yellow) and Tyr341 (blue). **B**) Observed binding mode of TH65 (orange sticks) in the catalytic pocket of smHDAC8 (white cartoon). Side chains of the smHDAC8 residues lining the pocket are shown as white sticks and the zinc ion as a purple sphere. Metal coordination is depicted as cyan-dashed lines, hydrogen bonds as yellow-dashed lines and cation-pi interactions as green-dashed lines. Water molecules are omitted.

We started our campaign by synthesizing structurally related derivatives of TH65 keeping firstly the biphenyl ring system, either as such or substituted, as the capping group while changing the substituents at position-4 of the benzhydroxamate moiety **(5a-f)**. These modifications resulted in the case of **5b, 5c** and **5d** in good inhibition of the recombinant parasitic enzyme. Compounds with substituted biphenyl ring system (**5c-f**) showed a decreased inhibitory activity against the human isoform. Best selectivity for smHDAC8 was observed for compound **5c** with a methoxy substituent in *o*-position to the amide linker. The chloro-substituent at the *o*-position of the capping group seems to be determinant for the increased selectivity for smHDAC8 over hHDAC8 (**Figure 3-A**). Docking studies in smHDAC8 reveal that the chloro-substituent in **5c** forces the capping group to slightly tilt toward the L6 loop. Nevertheless, the biphenyl capping group still undergoes various stabilizing interactions with the residues lining the side pocket including hydrophobic interactions between the chloro group and Tyr341, pi-pi stacking interactions between the phenyl group and His292, as well as van-der-Waals interactions between the terminal phenyl group and Pro291 (**Figure 3-A**). In the human HDAC8 isoform, the predicted binding mode reveals that the capping group does not protrude into the HDAC8-specific pocket but is rather placed on top of the L6 loop. The interaction, which is usually observed between the capping group of this class of compounds with Tyr306, cannot be observed, and the capping group only shows van-der-Waals interactions with the gatekeeper residue Met274 (**Figure 3-B**). Apart from **5a**, which showed potent inhibition of hHDAC6, the compounds showed only micromolar inhibition against hHDAC1 and 6 **(Table 1)**.

The next modification of the capping group was achieved by changing the biphenyl ring system and introduction of an ether linkage **(19a and 19b)**. The compounds showed a less potent inhibition against smHDAC8. Introduction of further chloro substituents at the terminal phenyl ring (**19c)** did not show a significant impact on the schistosomal enzyme, but decreased the activity on the human isoform

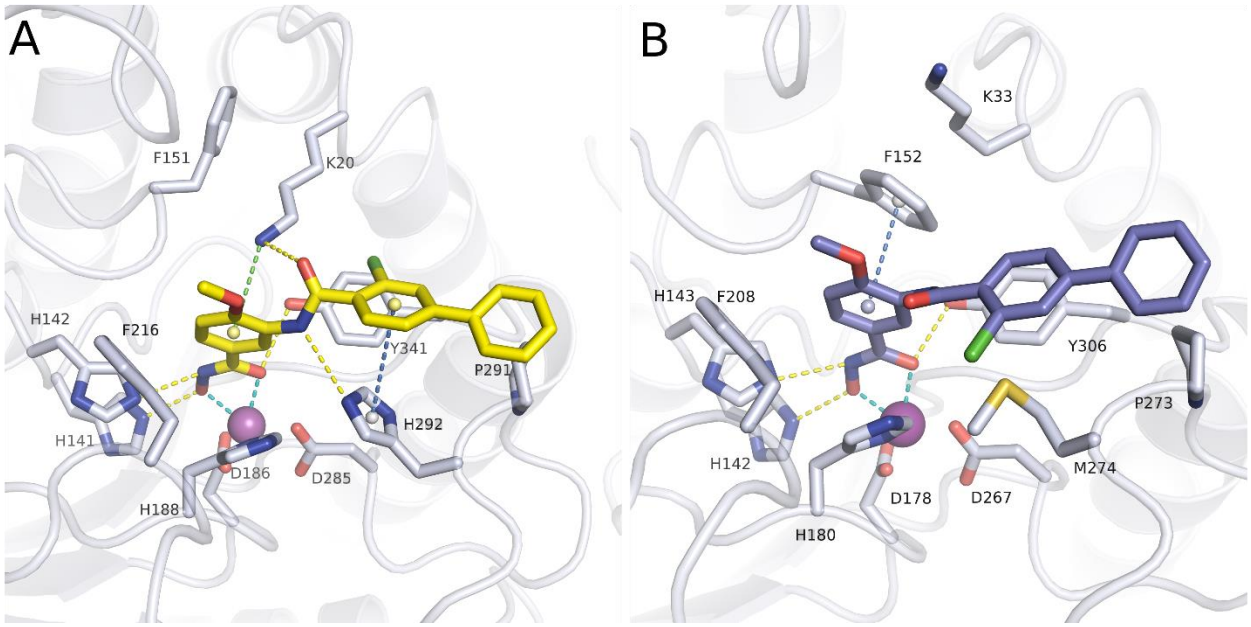

Figure 3: Docking poses of **5c** in smHDAC8 and hHDAC8. **A**) Predicted binding mode of **5c** (yellow sticks) in smHDAC8 (PDB ID 6HTH), **B**) Obtained docking pose of **5c** (purple sticks) in hsHDAC8 (PDB ID 2V5X). Side chains of the active site residues lining the pocket of smHDAC8 and hsHDAC8 are shown as white sticks. The zinc ion is displayed as a purple sphere. Metal coordination is depicted as cyan-dashed lines, hydrogen bonds as yellow-dashed lines, cation-pi interactions as green-dashed lines and pi-pi stacking interactions as blue-dashed lines. Water molecules are omitted.

We then tried a simplified capping group, namely one phenyl ring with different substitution patterns. Substitutions by different alkoxy groups at position-4 of the phenyl capping group **(5g-i)** led to a decrease in the activity on smHDAC8, albeit the compounds still showed submicromolar inhibitory potency. Interestingly, 2,4 dimethoxy substitution **(5j)** of the phenyl capping group led to a sharp decrease in the activity. The combination of a more bulky ethoxy substituent next to the amide linker and a 2,4-dichloro substitution of the terminal aromatic ring **(5k)** restored the activity against both parasitic and hHDAC8, while showing good selectivity against HDACs 1 and 6.

Finally, the introduction of an acetyl moiety in the capping group led to the highly potent smHDAC8 inhibitor **5l.** It was therefore chosen for further derivatization to obtain more selective derivatives.

Table 1: Chemical structures and in vitro results for benzhydroxamates

ID	Structure	IC_{50} µM smHDAC8	IC_{50} µM hHDAC8	IC_{50} µM hHDAC1	IC_{50} µM hHDAC6
5a	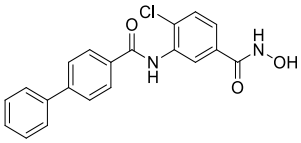	0.40 ± 0.09	0.45 ± 0.08	10.87 ± 1.52	0.16 ± 0.03
5b	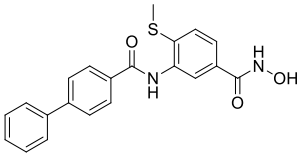	0.10 ± 0.01	0.22 ± 0.05	3.88 ± 0.32	1.50 ± 0.09
5c	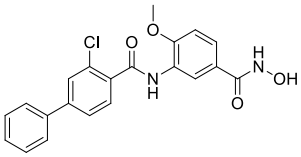	0.10 ± 0.08	1.10 ± 0.23	16 ± 6 % @ 10 µM n.i. @ 1 µM	46 ± 7 % @ 10 µM 15 ± 5 % @ 1 µM
5d	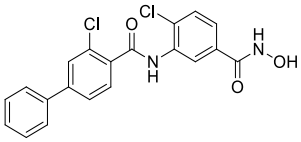	0.11 ± 0.01	0.78 ± 0.19	18 ± 2 % @ 10 µM 7 ± 2 % @ 1 µM	2.4 ± 0.3
5e	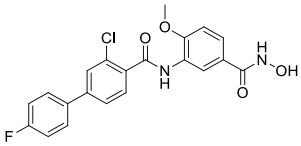	0.32 ± 0.02	48 ± 5 % @ 1 µM	n.d.	n.d.
5f	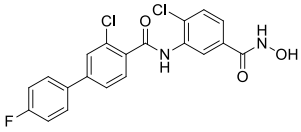	0.28 ± 0.04	25 ± 2 % @ 1 µM	n.d.	n.d.
19a	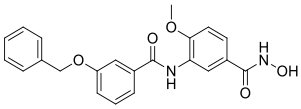	0.61 ± 0.07	59 ± 3 % @ 1 µM	n.d.	n.d.
19b	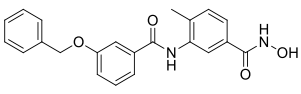	0.45 ± 0.03	60 ± 4 % @ 1 µM	n.d.	n.d.
19c	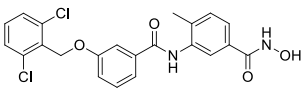	0.52 ± 0.02	34 ± 2 % @ 1 µM	n.d.	n.d.

5g	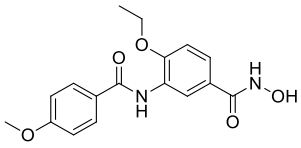	51 ± 3 % @ 0.5 µM	n.d.	n.d.	n.d.
5h	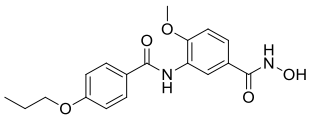	0.73 ± 0.09	66 ± 5 % @ 1 µM	n.d.	n.d.
5i	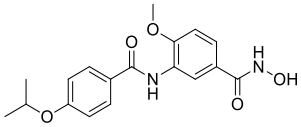	0.73 ± 0.05	58 ± 5 % @ 1 µM	n.d.	n.d.
5j	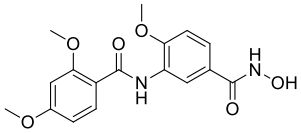	2.08 ± 0.27	63 ± 4 % @ 1 µM	n.d.	n.d.
5k	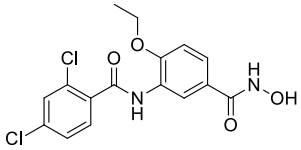	0.10 ± 0.01	0.23 ± 0.04	21.1 ± 2.3	7.74 ± 0.57
5l	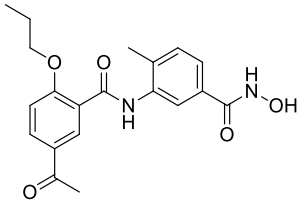	0.11 ± 0.02	0.14 ± 0.02	0.36 ± 0.03	0.02 ± 0.002
TH65		0.29 ± 0.04	0.13 ± 0.05	6.34 ± 2.10	0.39 ± 0.002
SAHA		1.56 ± 0.20	0.40 ± 0.10	0.12 ± 0.01	0.04 ± 0.01
PCI34051		0.44 ± 0.06	0.01 ± 0.003	48 ± 4 % @ 100 µM	41± 4 % % @ 100 µM

Based on the crystal structure of smHDAC8/TH65, one suggested modification of the capping group was to replace the biphenyl ring system with polycyclic rings to address the hydrophobic HDAC8-specific pocket **(Table 2)**. Therefore, we used bicyclic rings (**5m** and **5n**) and observed that the nanomolar inhibition of smHDAC8 was retained, accompanied with a potent activity on hHDAC6 and 8. Molecular docking studies of **5n** revealed that the bicyclic capping group occupies the hydrophobic side pocket of smHDAC8 showing pi-pi stacking interactions with Tyr341 as well as hydrophobic interactions with Pro291 and His292. (**Figure 4-A**). In human

HDAC8, docking studies showed that the compounds can adopt a similar binding conformation as observed in smHDAC8. The bicyclic capping group occupies the side pocket showing pi-pi stacking interactions with Tyr306 as well as hydrophobic interactions with Pro273 and Met274 (**Figure 4-B**).

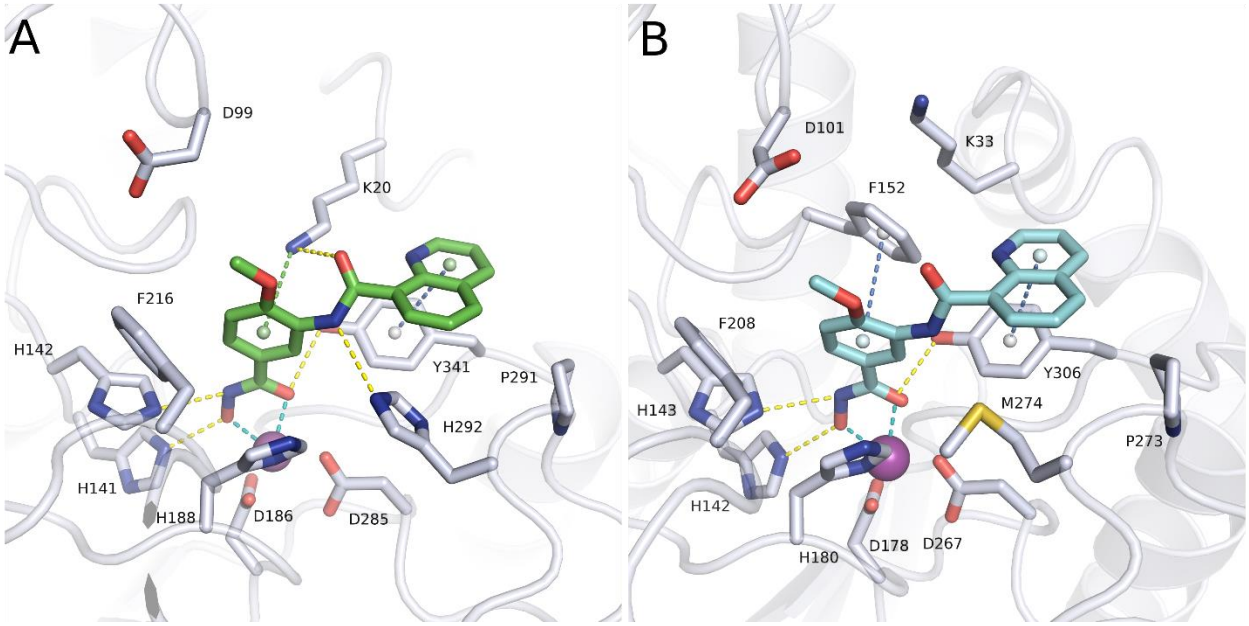

Figure 4: Binding modes of the bicyclic derivative **5n**. **A**) Predicted binding modes of **5n** (green sticks) in smHDAC8 (PDB ID 6HTH, white sticks); **B**) Predicted binding modes of **5n** (cyan sticks) in hsHDAC8 (PDB ID 2V5X). The zinc ion is displayed as a purple sphere. Metal coordination is depicted as cyan-dashed lines, hydrogen bonds as yellow-dashed lines, cation-pi interactions as green-dashed lines and pi-pi stacking interactions as blue-dashed lines

We next turned to tri-heterocyclic rings (**5o**) which showed a comparable potent activity on both parasitic and human HDAC8. In addition, we aimed to synthesize further analogues bearing different bioisosteres of the dibenzofuran ring. **5p** and **24** exhibited comparable inhibitory activity to **5o** against sm- and hHDAC8. Similar to **5n**, the tricyclic moiety of **5o** was found to be embedded in the hydrophobic side pocket of smHDAC8, displaying aromatic and hydrophobic interactions with Tyr341, Pro 291 and His292 (**Figure 5-A**). A similar binding mode was also observed for the analogous tricyclic derivatives **5p** and **24** in smHDAC8 (**Figure 5-B**). Docking studies in the human HDAC8 isoform also revealed that the tricyclic capping group can be well accommodated in the hydrophobic side pocket, where it is stabilized by interactions with Tyr306, Pro273, and Met274 (**Figure 5-C**). Meanwhile, in HDAC6 the capping group resides above L1 and L6 loops, showing hydrophobic interactions with Pro501 and Leu749 (**Figure 5-D**). As previously observed for other m-substituted derivatives, **5o** is not able to properly chelate the catalytic zinc ion in HDAC1, which explains its low HDAC1-inhibitory activity (**Figure S2-Supplementary**). Moreover, based on our previous work, where we reported that hydroxamates

with an amine linker are potent hHDAC8 inhibitors [36], we synthesized a close analogue of **5o**, where we replaced the amide linker with an amine one to get **8**. The compound showed almost half the activity of its amide analogues against both sm- and hHDAC8, but still in the nanomolar range.

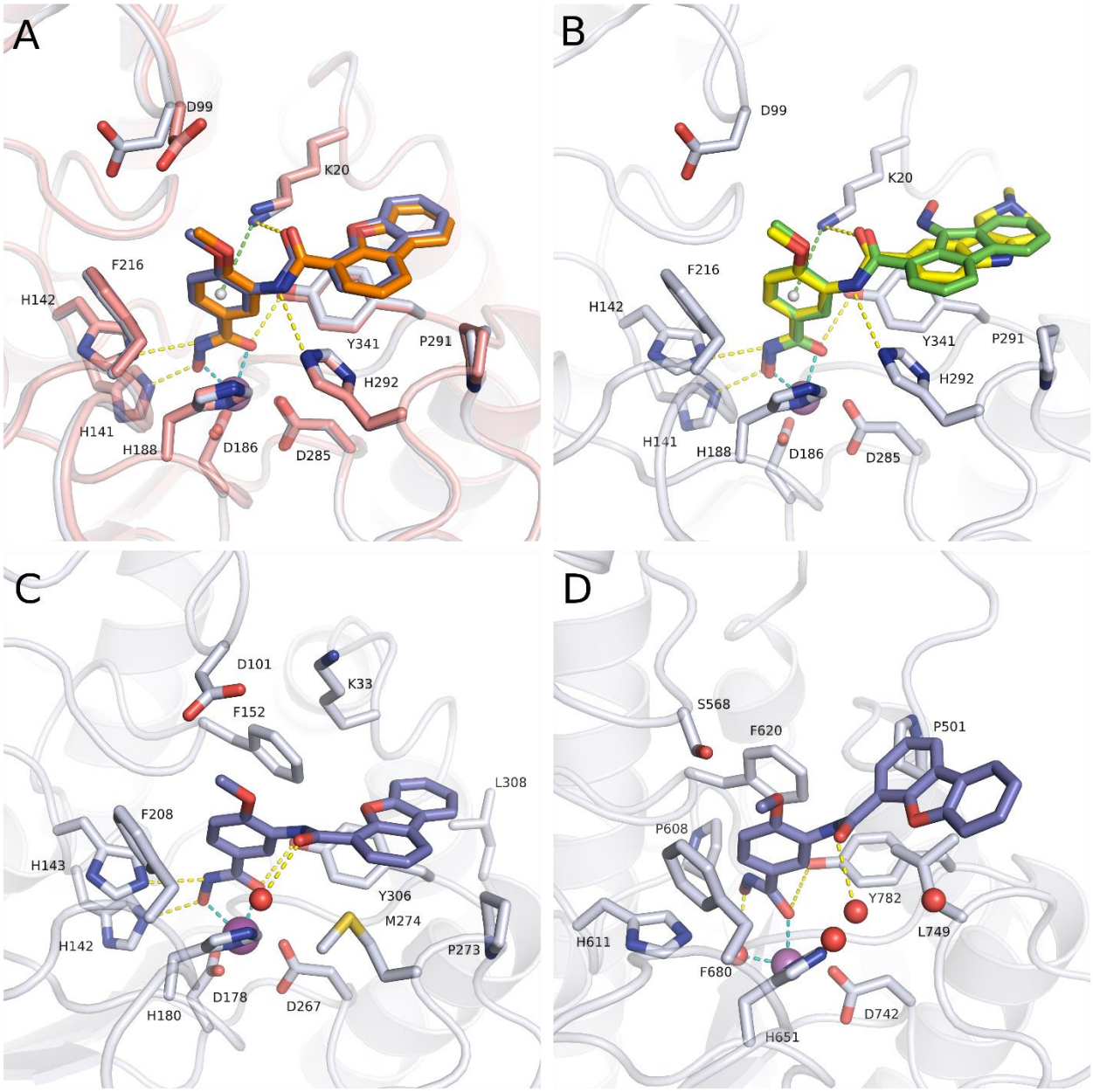

Figure 5: Binding modes of the tricyclic derivatives. **A**) Docking pose of **5o** (purple-blue sticks) in smHDAC8 (PDB ID 6HTH, white sticks) overplayed with the experimentally determined binding mode of **5o** (PDB ID 7P3S, orange sticks) in smHDAC8 (salmon sticks); **B**) Predicted binding modes of the **24** (yellow sticks) and **5p** (green sticks) in smHDAC8 (PDB ID 6HTH); **C**) Predicted binding mode of **5o** (purple-blue sticks) in hsHDAC8 (PDB ID 2V5X); **D**) Predicted binding mode of **5o** (purple-blue sticks) in hsHDAC6 (PDB ID 5EDU). The zinc ion is displayed as a purple sphere. Metal coordination is

depicted as cyan-dashed lines, hydrogen bonds as yellow-dashed lines, and cation-pi interactions as green-dashed lines.

Table 2: Chemical structures and *in vitro* results for benzhydroxamates containing bi- and tricyclic capping groups

ID	Structure	IC_{50} µM smHDAC8	IC_{50} µM hHDAC8	IC_{50} µM hHDAC1	IC_{50} µM hHDAC6
5m	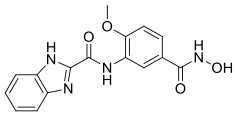	0.58 ± 0.07	29 ± 3 % @ 1 µM	n.d.	n.d.
5n	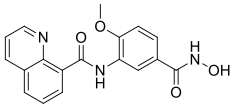	0.33 ± 0.05	0.18 ± 0.04	n.d.	n.d.
5o	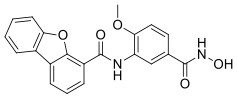	0.27 ± 0.02	0.32 ± 0.03	18.51 ± 1.60	0.29 ± 0.07
24	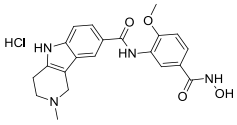	0.20 ± 0.02	0.29 ± 0.03	n.d.	n.d.
5p	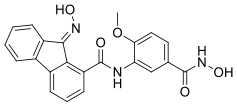	0.32 ± 0.03	0.15 ± 0.03	n.d.	n.d.
8	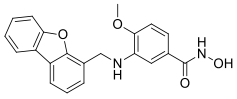	0.45 ± 0.09	0.86 ± 0.13	n.d.	n.d.

We previously showed that inhibitors with inverted amide linker are potent HDAC8 inhibitors. [36] We hypothesized then that these "inverse amides" could also inhibit the parasitic enzyme. As a proof of concept, we firstly tested our previously reported hHDAC8 inhibitors **(13a-c)** on smHDAC8, and the inhibitors indeed showed a potent inhibition of the parasitic enzyme in the nanomolar range. As mentioned above, compound **5l** bearing the acetyl moiety showed a potent inhibition against smHDAC8 as well as hHDACs1,6 and 8. We then aimed to prepare another set of inhibitors **(13d-j)** where we inverted the amide linker of **5l** to benefit from the HDAC8 inhibitory activity of the inverse amides. In the cases of **13d** and **13e** we observed potent inhibition of smHDAC8 and slight selectivity against hHDAC8 (**Table 3**). With the need to improve the selectivity of the compounds, we synthesized further inverse amides lacking the acetyl group at the capping group **(13k-n)**. Simple mono- and disubstituted phenyl rings bearing methoxy and chloro substituents as well as a bicyclic benzothiophene ring were included. Interestingly these inhibitors retained the nanomolar activity against the parasitic and human HDAC8 while showing decreased inhibition of hHDAC1 and 6.

A more detailed study describing all docking results, binding free energy calculations, as well as the generation of quantitative structure activity relationship (QSAR) models of the developed smHDAC8 inhibitors that have been used in combination to the chemical optimization has been published elsewhere [37].

Table 3: Chemical structures and in vitro results for benzhydroxamates with inverse amide linker

ID	R	IC_{50} µM smHDAC8	IC_{50} µM hHDAC8	IC_{50} µM hHDAC1	IC_{50} µM hHDAC6
13a	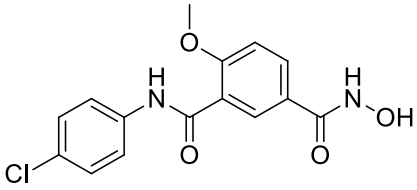	0.31 ± 0.07	0.04 ± 0.002	n.d.	n.d.
13b	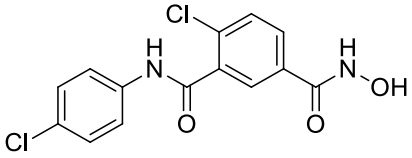	60 ± 3 % @ 1 µM	0.18 ± 0.05	20 ± 1 % @ 1 µM	94 ± 4 % @ 1 µM
13c	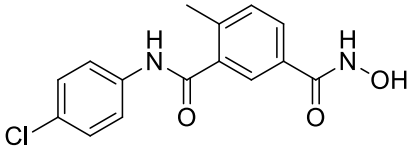	0.33 ± 0.04	0.11 ± 0.01	3.37 ± 0.63	0.60 ± 0.04
13d	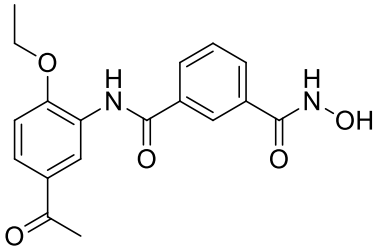	0.16 ± 0.02	0.59 ± 0.09	7.7 ± 1.5	0.12 ± 0.016
13e	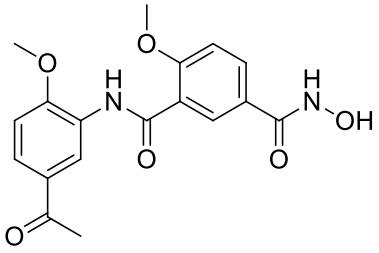	0.15 ± 0.02	71 ± 4 % @ 1 µM	0.36 ± 0.25	0.02 ± 0.002

13f	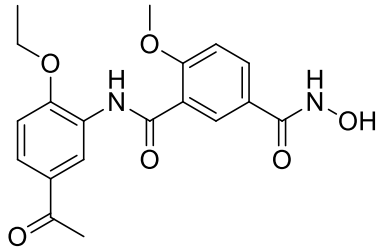	0.33 ± 0.03	61 ± 5 % @ 1 µM	n.d.	n.d.
13g	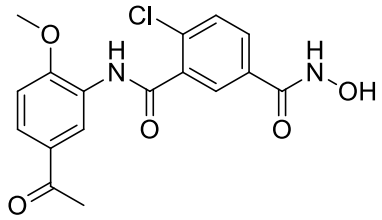	0.29 ± 0.03	0.09 ± 0.01	n.d.	n.d.
13h	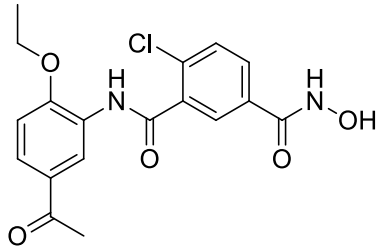	0.14 ± 0.02	0.22 ± 0.04	18.1 ± 6.2	0.11 ± 0.02
13i	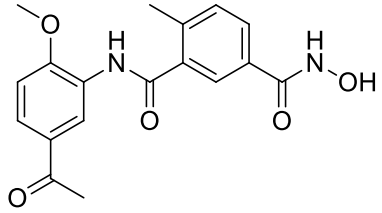	0.18 ± 0.03	0.09 ± 0.01	n.d.	n.d.
13j	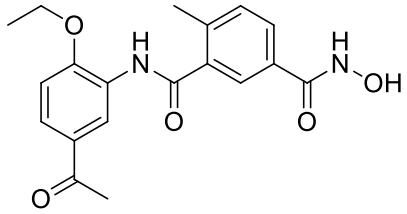	0.21 ± 0.02	0.07 ± 0.004	n.d.	n.d.
13k	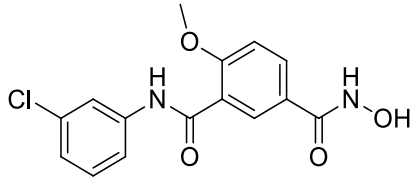	0.17 ± 0.01	0.28 ± 0.04	0 ± 1 % @ 1 µM	25 ± 2 % @ 1 µM
13l	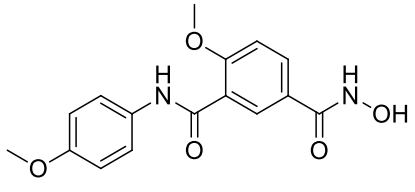	0.43 ± 0.02	0.27 ± 0.05	2 ± 1 % @ 1 µM	18 ± 2 % @ 1 µM

13m	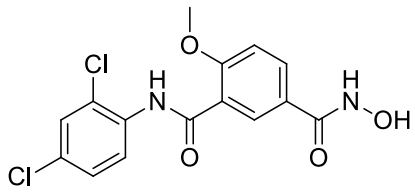	0.18 ± 0.0	31 ± 3 % @ 1 µM	n.d.	n.d.
13n	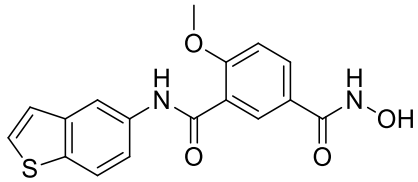	0.22 ± 0.02	0.10 ± 0.01	n.d.	n.d.

3. Crystallographic studies

To confirm the docking results of the new inhibitors, the crystal structure of smHDAC8 in complex with **5o** (**Figure 5-A**) was solved and refined at 1.55 Å (**Table S3 and Figure S4-Supplementary**). The crystal structure showed that **5o** binds in the active site, where it coordinates with the catalytic zinc ion, and the tricyclic capping group was found to be embedded in the hydrophobic side pocket of smHDAC8, displaying aromatic and hydrophobic interactions with Tyr341, Pro 291 and His292, as predicted by the docking study. The interaction is similar to our previously solved crystallographic structures with other compounds [35].

4. Chemistry

The compounds in the present work were synthesized through 5 schemes. Apart from compound **24** (illustrated in scheme **5**), the synthetic strategy aimed to get the carboxylic acid intermediates **(4a-b**, **7**, **12a-n** and **18a-c)**, converted then to the corresponding hydroxamates through the well-established method by amide coupling with O-(Tetrahydro-2*H*-pyran-2-yl)hydroxylamine followed by acidic deprotection [38]. Scheme **1** illustrates the synthesis of compounds **(5a-p)**, where amide coupling followed by basic hydrolysis afforded the required carboxylic acid intermediates **(4a-b)**. While carboxylic acids **(4a-o)** were smoothly converted to the corresponding hydroxamates, 4-methoxy-3-(9-oxo-9*H*-fluorene-1-carboxamido)benzoic acid **4p** gave unexpected product *N*-[5-(hydroxycarbamoyl)-2-methoxyphenyl]-9-(hydroxyimino)-9*H*-fluorene-1-carboxamide **5p** instead of the originally wanted compound *N*-[5-(hydroxycarbamoyl)-2-methoxyphenyl]-9-oxo-9*H*-fluorene-1-carboxamide. This could be explained – as shown in **Figure 6** – that the THP protected hydroxylamine reacted not only with the activated acid (to produce the THP protected hydroxamic acid), but also with the carbonyl group in a condensation reaction to give the corresponding ketoxime. Deprotection with HCl removed both THP groups yielding compound **5p**.

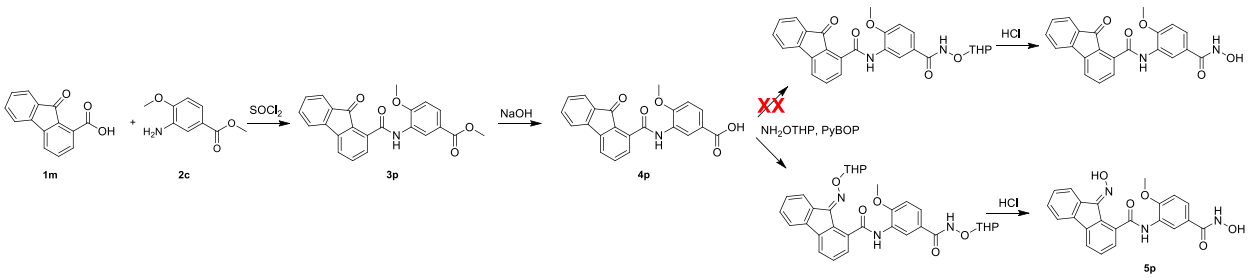

Figure 6: predicted pathway for the synthesis of unexpected compound **5p**.

As shown in scheme 2, reductive amination afforded directly the key carboxylic acid intermediate **7**, while again amide coupling followed by alkaline hydrolysis yielded carboxylic acids **(12a-n)** used to synthesize the inverse amide hydroxamates **(13a-n)** as illustrated in scheme **3**. In scheme **4**, Williamson ether synthesis was utilized to build the ether bond with subsequent amide bond formation and hydrolysis to yield intermediates **(18a-c)**. Although compound **24** is structurally related to compounds **(5a-p)**, trials to synthesize it in a similar sequence as in scheme **1** didn't succeed due to its high polarity that interfered with the purification of the intermediates. Therefore a slightly modified synthetic sequence was adopted – as shown in scheme **5** – where the THP protected intermediate **20** was first synthesized, coupled to carboxylic acid **23**, and finally deprotected to give the final compound **24**.

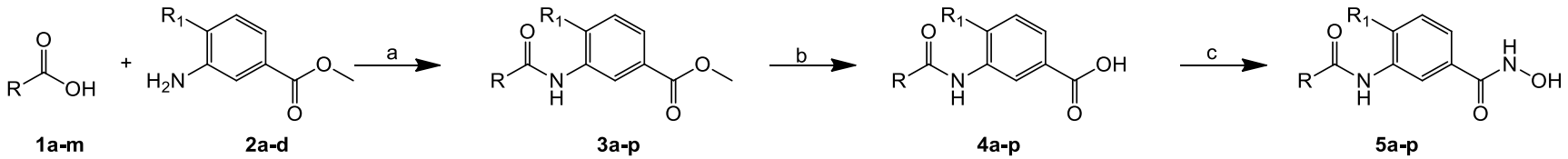

Scheme 1: Reagents and conditions: (a) i) thionyl chloride, reflux, ii) DIPEA, THF; (b) i) aqu. NaOH, Methanol, reflux, ii) dil. HCl; (c) i) PyBOP, DIPEA, H_2NOTHP, THF, ii) dil. HCl, THF.

ID	R	R_1	ID	R	R_1	ID	R	R_1
5a	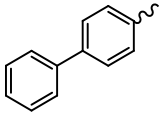	Cl	**5g**	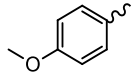	OCH_2CH_3	**5m**	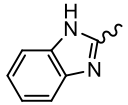	OCH_3
5b	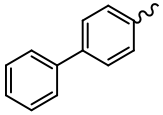	SCH_3	**5h**	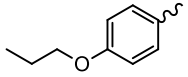	OCH_3	**5n**	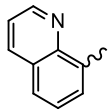	OCH_3
5c	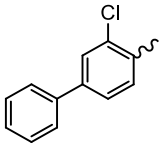	OCH_3	**5i**	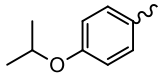	OCH_3	**5o**	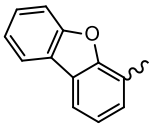	OCH_3
5d	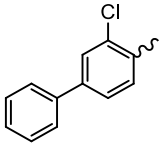	Cl	**5j**	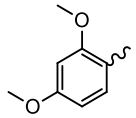	OCH_3	**5p**	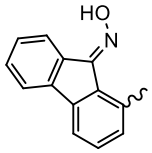	OCH_3
5e	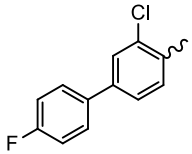	OCH_3	**5k**	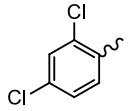	OCH_2CH_3			

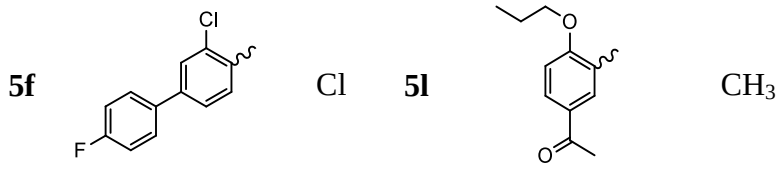

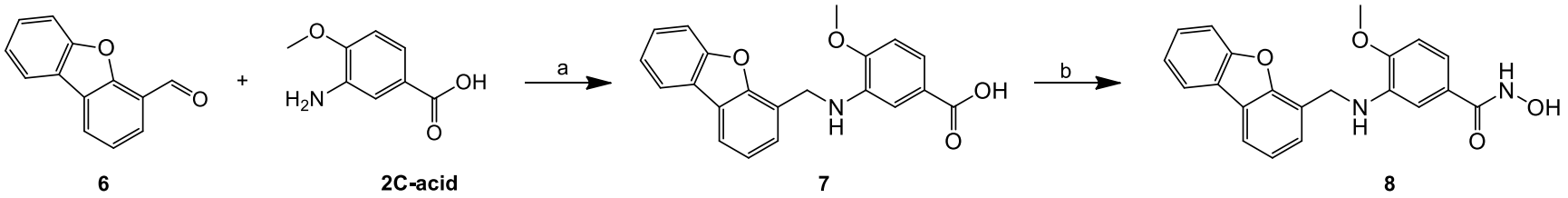

Scheme 2: Reagents and conditions: (a) i) $Na(AcO)_3BH$, acetic acid, THF; (b) i) PyBOP, DIPEA, H_2NOTHP, THF, ii) dil. HCl, THF.

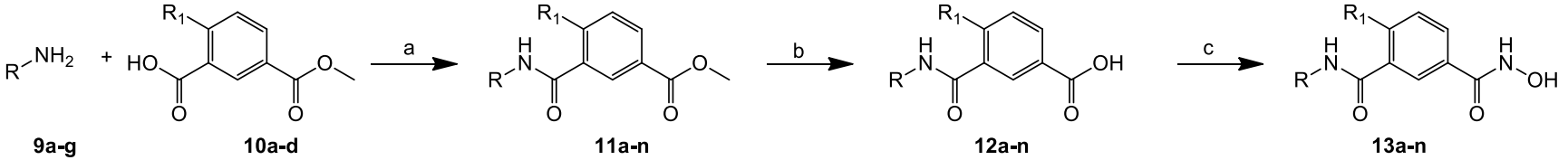

Scheme 3: Reagents and conditions: (a) i) oxalyl chloride, cat. DMF, dichloromethane, ii) DIPEA, dichloromethane; (b) i) aqu. NaOH, Methanol, reflux, ii) dil. HCl; (c) i) PyBOP, DIPEA, H_2NOTHP, THF, ii) dil. HCl, THF.

ID	R	R_1	**ID**	R	R_1	**ID**	R	R_1
13a	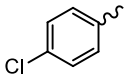	OCH_3	**13f**	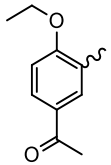	OCH_3	**13k**	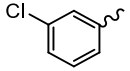	OCH_3

13b	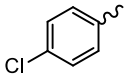	Cl	**13g**	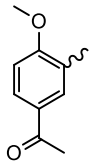	Cl	**13l**	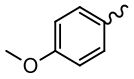	OCH_3
13c	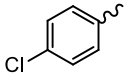	CH_3	**13h**	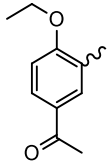	Cl	**13m**	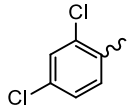	OCH_3
13d	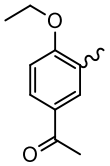	H	**13i**	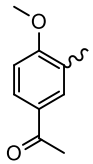	CH_3	**13n**	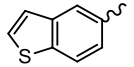	OCH_3
13e	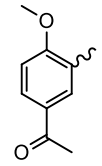	OCH_3	**13j**	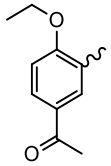	CH_3			

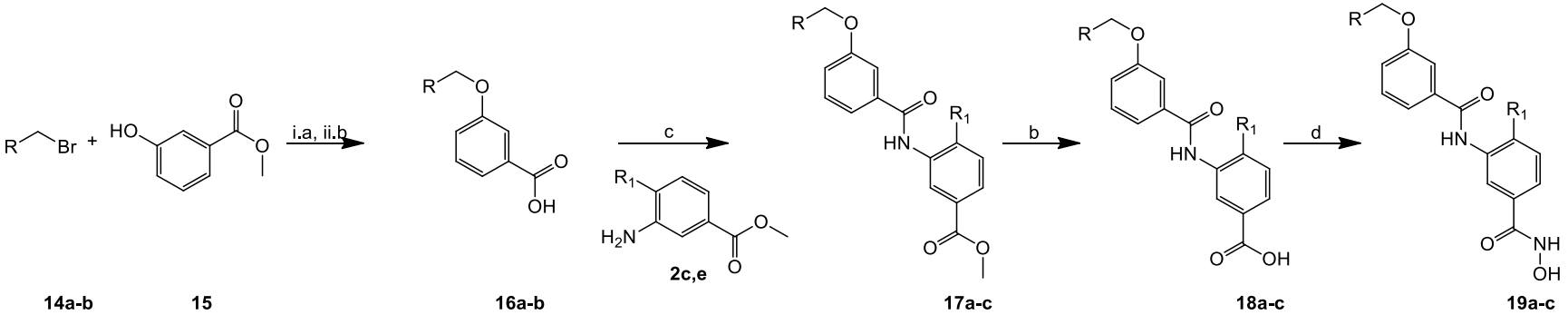

14a-b **15** **16a-b** **17a-c** **18a-c** **19a-c**

Scheme 4: Reagents and conditions: (a) K_2CO_3, DMF, RT; (b) i) aqu. NaOH, Methanol, reflux, ii) dil. HCl; (c) i) Thionyl chloride, reflux, ii) DIPEA, THF; (d) i) PyBOP, DIPEA, H_2NOTHP, THF, ii) dil. HCl, THF.

ID	R	R_1	ID	R	R_1	ID	R	R_1
19a		OCH_3	**19b**		CH_3	**19c**	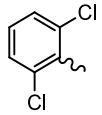	CH_3

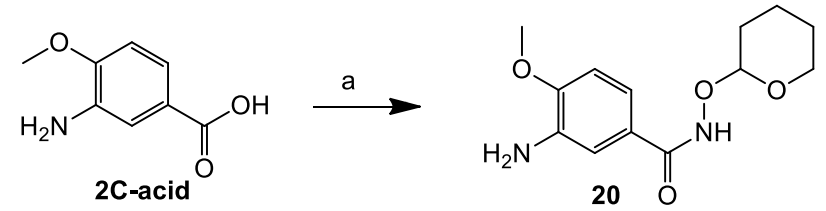

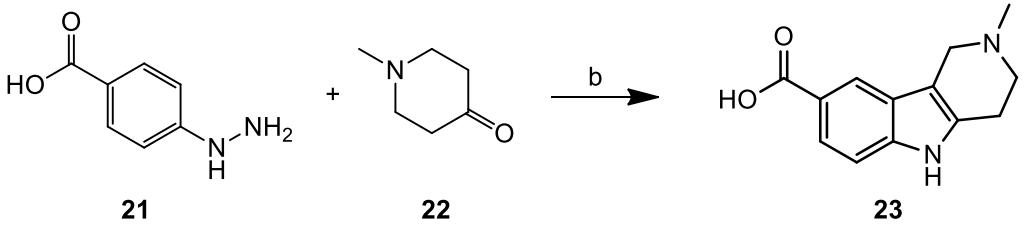

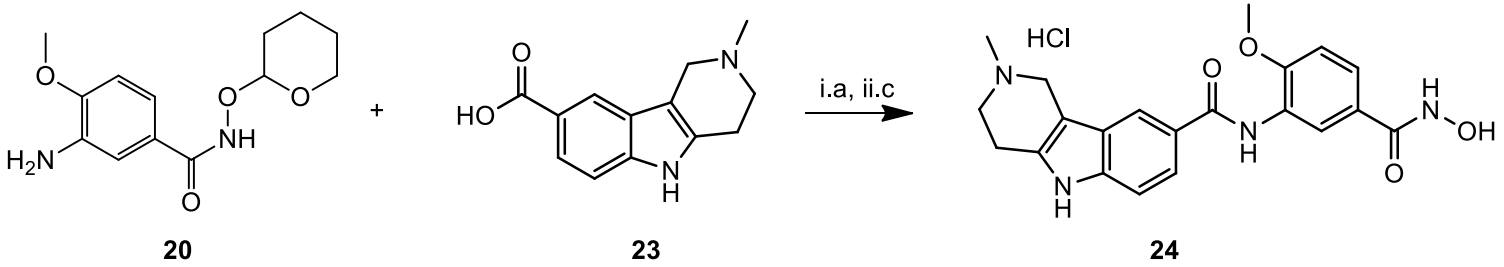

Scheme 5: Reagents and conditions: (a) PyBOP, DIPEA, H_2NOTHP, THF; (b) i) conc. HCl, Dioxane, reflux, ii) dil. NaOH; (c) dil. HCl, THF.

5. Phenotypic screening on schistosomula

We next analyzed the effect of the developed compounds on the parasites maintained in culture. The compounds were initially tested for their toxicity toward *S. mansoni* schistosomula using an Alamar Blue-based viability assay (see Experimental Methods). Initial testing was done at a concentration of 10 µM and selected compounds were also tested at 20 µM in order to determine dose-dependency. Two biological replicates were carried out in triplicate and the results are shown in **Table 4**. In addition to the compounds developed during this study, the previously developed smHDAC8 inhibitors TH65, the reported HDAC8 selective inhibitor PCI-34051 and Praziquantel, the drug used for treating schistosomiasis, were also included in the assay. Many of the tested compounds showed toxic effects towards the parasite comparable to the reference TH65. Nevertheless, some synthesized inhibitors were even more potent, such as **19c, 5l, 13h** and **13j**. However, it was **5o** which provoked the most marked dose-dependent reductions in schistosomula viability, killing almost 98% of the schistosomula. In this assay PCI-34051 showed only very modest activity against schistosomula and as expected, Praziquantel was inactive at the concentrations used. In view of the primary assay data and its selectivity of inhibition with regard to human HDAC1, **5o** was chosen for further testing. We first showed that the EC_{50} value for this compound using the Alamar Blue-based assay was 3.5 µM **(Figure 7)** on schistosomula after 72 hours in culture. Taking into consideration the potent EC_{50} value of **5o**, we were then interested to test this compound *in vivo* in mice infected with *S. mansoni*. However, due to its lipophilicity and poor solubility, all our trials to prepare a formulation to solubilize the amount required for the *in vivo* testing were unsuccessful (data not shown). To overcome that, we designed and synthesized its analogue **24** as a hydrochloride salt. This derivative was indeed better soluble and showed almost the same activity on smHDAC8, but unfortunately it showed a negligible toxicity toward the schistosomula. A general observation from our work on *S. mansoni* was that the more lipophilic inhibitors were the most potent in the phenotypic screening, most likely due to increased permeability into the parasite. A good balance between lipophilicity and water solubility is therefore critical for these inhibitors to be advanced to in vivo testing.

Table 4: Toxicity Studies on *S. mansoni* Schistosomula (Alamar Blue Assay) and Cytotoxicity Studies in HEK293 Cells

	% viability *S. mansoni* 10 µM (n=2x3)	**% viability *S. mansoni* 20 µM (n=2x3)**	**% viability HEK293 50 µM (n=3)**
	Alamar Blue	**Alamar Blue**	**Alamar Blue**
TH65	64.8 ± 3.5	33.4 ± 3.5	12.3 ± 0.9*
5a	62.3 ± 0.9	55.1 ± 1.1	81.7 ± 2.6
5b	57.4 ± 6.8	64.9 ± 5.8	82.3 ± 1.9

5c	64.0 ± 4.6	65.6 ± 10.1	94.6 ± 1.6
5d	60.6 ± 2.9	43.5 ± 2.6	77.0 ± 1.7
5e	74.6 ± 6.0	60.5 ± 5.6	83.5 ± 3.2
5f	63.4 ± 6.1	56.6 ± 8.3	82.2 ± 3.0
19a	61.0 ± 4.7	56.2 ± 8.0	95.4 ± 1.6
19b	67.3 ± 2.0	46.5 ± 8.4	81.4 ± 6.4
19c	38.4 ± 2.6	22.3 ± 2.1	66.6 ± 4.4
5g	64.4 ± 2.0	59.4 ± 0.6	88.7 ± 0.9
5h	70.7 ± 9.4	51.6 ± 1.1	93.2 ± 2.0
5i	72.6 ± 3.0	56.2 ± 4.8	93.1 ± 1.8
5j	65.3 ± 1.6	66.5 ± 6.7	88.4 ± 1.6
5k	56.2 ± 2.3	56.4 ± 0.1	86.8 ± 2.1
5l	45.2 ± 1.6	34.0 ± 3.9	68.8 ± 2.8
5m	69.5 ± 6.6	47.1 ± 8.1	83.5 ± 1.4
5n	62.0 ± 0.4	40.0 ± 1.5	77.0 ± 9.8
5o	2.2 ± 1.1	n.d.	73.0 ± 5.7
24	98.0 ± 0.3	100.0 ± 0.5	71.1 ± 1.7
5p	98.5 ± 3.4	96.0 ± 5.5	76.6 ± 5.9
13a	77.3 ± 3.0	59.2 ± 3.2	27.5 ± 0.8
13b	77.6 ± 5.0	62.3 ± 1.7	69.5 ± 3.8
13c	69.1 ± 2.7	50.2 ± 12.2	67.6 ± 3.7
13d	81.0 ± 0.9	67.3 ± 0.6	81.2 ± 13.5
13e	78.2 ± 1.7	66.2 ± 1.7	66.2 ± 3.7
13f	64.3 ± 4.0	56.7 ± 1.3	59.9 ± 4.8
13g	62.6 ± 4.8	32.3 ± 6.3	89.1 ± 5.5
13h	57.0 ± 4.5	33.1 ± 4.9	60.6 ± 2.9
13i	75.2 ± 5.7	69.5 ± 5.0	94.8 ± 7.4
13j	42.1 ± 3.3	37.0 ± 1.6	87.7 ± 13.6

13k	85.6 ± 4.0	82.8 ± 4.0	88.2 ± 4.5
13l	91.0 ± 9.1	83.3 ± 1.4	94.5 ± 7.8
13m	88.2 ± 5.4	83.4 ± 4.0	58.3 ± 5.5
13n	82.1 ± 1.0	77.1 ± 9.8	95.6 ± 11.5
PCI-34051	71.0 ± 1.1	62.3 ± 4.1	96.8 ± 2.1
Praziquantel	92.1 ± 8.0	88.9 ± 6.4	99.3 ± 4.1

* IC_{50} value for TH65 was determined to be 199 µM [34]

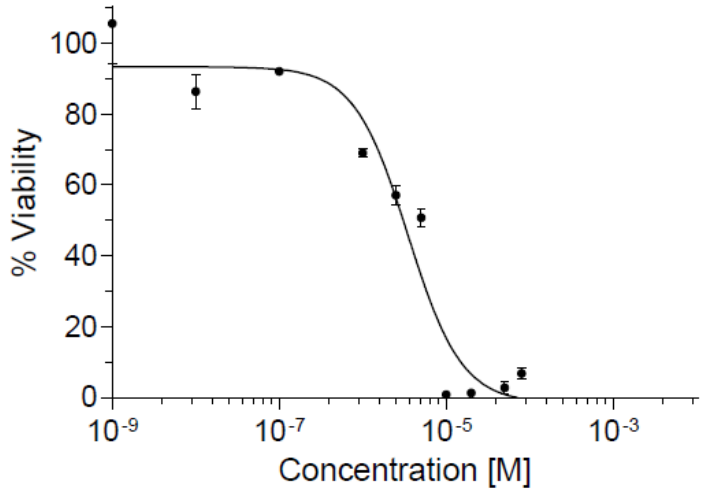

Figure 7. The activity on schistosomula shown as EC_{50}-value (3.5 µM) of compound **5o** using the Alamar Blue-based viability-assay.

6. Cytotoxicity study

Parasite-specific HDAC inhibitors should have low toxicity to mammalian cells. Therefore, we tested the potential cytotoxicity of the synthesized inhibitors in a human epithelial kidney cell line (HEK293). The cells were incubated for 48 h with the indicated compounds at a concentration of 50 µM, and cell viability was determined by Alamar Blue assay. The majority of the tested inhibitors showed only relatively low cytotoxicity in the human cell system used and were all less toxic than TH65 (**Table 4**).

7. Conclusion

In summary, we have designed, synthesized and tested in vitro several new benzhydroxamates as smHDAC8 inhibitors to further explore their SAR. In addition we performed docking and crystallization studies to increase our understanding of their interaction with the target enzyme as

well as other human orthologues. Many of the compounds developed in this work showed potent smHDAC8, mainly accompanied with comparable hHDAC8, and - apart from some exceptions - they showed decreased inhibition of hHDACs1,6. The developed inhibitors were then screened for their phenotypic activity against the schistosomula, and we have identified compound **5o** as the most potent one with EC_{50}-value of 3.5 µM. Due to the low solubility of **5o** we synthesized a more soluble bioisostere **24**, which retained the inhibitory activity. Unfortunately, **24** lacked cellular activity. We could also solve the crystal structures of **5o** in complex with smHDAC8, gaining detailed insights how this potent inhibitor, esp. the tricyclic capping group interacts with the parasitic enzyme (**Figure S4- Supplementary**). Finally, the developed compounds showed a good safety profile against human HEK293 cells.

8. Experimental protocols

8.1. Chemistry

8.1.1. General

All materials and reagents were purchased from Sigma-Aldrich Co. Ltd. and abcr GmbH. All solvents were analytically pure and dried before use. Thin layer chromatography was carried out on aluminum sheets coated with silica gel 60 F254 (Merck, Darmstadt, Germany). For column chromatography under normal pressure silica gel 60 (0.036−0.200 mm) was used.

Final compounds were confirmed to be of >95% purity based on HPLC. Purity was measured by UV absorbance at 254 nm. The HPLC consists of an XTerra RP18 column (3.5 µm, 3.9 mm × 100 mm) from the manufacturer Waters (Milford, MA, USA) and two LC-10AD pumps, a SPD-M10A VP PDA detector, and a SIL-HT autosampler, all from the manufacturer Shimadzu (Kyoto, Japan). For preparative tasks a XTerra RP18 column (7 µm, 19 mm × 150 mm) from the manufacturer Waters (Milford, MA, USA) and two LC-20AD pumps were used. The mobile phase was in all cases a gradient of methanol/ water (starting at 95% water going to 5% water).

Mass spectrometry analyses were performed with a Finnigan MAT710C (Thermo Separation Products, San Jose, CA, USA) for the ESIMS spectra and with a LTQ (linear ion trap) Orbitrap XL hybrid mass spectrometer (Thermo Fisher Scientific, Bremen, Germany) for the HRMS-ESI (high resolution mass spectrometry) spectra. For the HRMS analyses the signal for the isotopes with the highest prevalence was given and calculated (^{35}Cl, ^{79}Br).

^{1}H NMR and ^{13}C NMR spectra were taken on a Varian Inova 500 using deuterated chloroform and deuterated DMSO as solvent. Chemical shifts are referenced to the residual solvent signals. The following abbreviations and formulas for solvents and reagents were used: dimethylformamide (DMF), dimethylsulfoxide (DMSO), tetrahydrofuran (THF), N,N-diisopropylethylamine (DIPEA) and hydrochloric acid (HCl)

8.1.2. General synthetic methods

Method A, synthesis of amide bond using oxalyl chloride

The appropriate carboxylic acid (1 eq.), DMF (one drop) and oxalyl chloride (1.3 eq.) were stirred in dichloromethane at room temperature for 3 hours. The mixture was then added dropwise to a solution of the appropriate amine (0.9 eq.) and DIPEA (3 eq.) in dichloromethane, and stirring was continued for another 2 hours at room temperature. The reaction mixture was washed with a saturated aqueous solution of ammonium chloride and brine. The organic layer was dried over anhydrous sodium sulfate, filtered, and concentrated in vacuo. The residue was purified using column chromatography (chloroform / methanol as eluents). The yields were around 60-80%.

Method B, synthesis of amide bond using thionyl chloride

The appropriate carboxylic acid (1 eq.) was cooled to 0 °C and then thionyl chloride (2 eq.) was added dropwise. The mixture was then heated under reflux for 2 hours, and the excess of thionyl chloride was evaporated under vacuum. The acid chloride was dissolved in dry THF and added dropwise to a solution of the appropriate amine (0.9 eq.) and DIPEA (3 eq.) in THF. After completion, the reaction mixture was diluted with ethyl acetate and washed with a saturated aqueous solution of ammonium chloride and brine. The organic layer was dried over anhydrous sodium sulfate, filtered, and concentrated in vacuo. The residue was purified using column chromatography (chloroform / methanol as eluents). The yields were around 50-70%.

Method C, synthesis of amide bond using PyBOP

To a mixture of the appropriate carboxylic acid (1 eq.) and PyBOP (1.2 eq.) in DMF was added a solution of the appropriate amine (0.9 eq.) and DIPEA (3 eq.) in DMF. The reaction mixture was stirred at room temperature for 4-5 hours, then diluted with ethyl acetate and washed with a an aqueous solution of sodium hydroxide and brine. The organic layer was dried over anhydrous sodium sulfate, filtered, and concentrated in vacuo. The residue was purified using column chromatography (chloroform / methanol as eluents). The yields were around 60-70%.

Method D, reductive amination

A mixture of the appropriate aldehyde (1 eq.) and amine (0.9 eq.) was dissolved in toluene, and the reaction mixture was refluxed for 2 h using a dean stark apparatus. The solvent was then evaporated under reduced pressure, and the crude product was dissolved in THF and cooled to 0 °C. Sodium triacetoxyborohydride (3 eq.) was then added and the reaction mixture was stirred overnight at room temperature. The reaction was quenched by adding water and extracted with ethyl acetate. The organic layer was dried over anhydrous sodium sulfate, filtered, and concentrated in vacuo. The residue was purified using column chromatography (chloroform / methanol as eluents). The yields were around 60-70%.

Method E, synthesis of ether bond (Williamson ether synthesis)

To a suspension of the appropriate phenol (1 eq.) and potassium carbonate (3 eq.) in DMF was added the appropriate alkyl bromide (1.5 eq.), and the mixture was stirred at room temperature overnight. The reaction was quenched by adding water and extracted with ethyl acetate. The organic layer was dried over anhydrous sodium sulfate, filtered, and concentrated in vacuo. The residue was purified using column chromatography (n-hexane / ethyl acetate as eluents). The yields were around 70-80%.

.

Method F, ester hydrolysis

The appropriate methyl esters (1 eq.) was dissolved in methanol followed by the addition of aqueous solution of sodium hydroxide (10 eq.) and the mixture was stirred under reflux for 2-4 hours until complete hydrolysis of the ester. Methanol was then evaporated and the reaction was neutralized with aqueous solution of 1M HCl until pH 6. The liberated free acid was extracted with a mixture of ethyl acetate and THF, and the organic layer was dried over anhydrous sodium sulfate, filtered, and concentrated in vacuo to yield the product, which required no further purification. Crude yields were around 80-90%.

Method G, synthesis of hydroxamic acids

The appropriate carboxylic acid (1 eq.) was dissolved in dry THF, followed by the addition of PyBOP (1.2 eq.) and DIPEA (3 eq.). The mixture was stirred for 15 min, then NH_2OTHP (1.2 eq.) was added and the reaction mixture was stirred at room temperature for 2-4 hours. The solvent was evaporated under vacuum and the mixture was dissolved in ethyl acetate (50 ml) and washed with 1M sodium carbonate solution and brine. The organic layer was evaporated under vacuum and the product was purified by column chromatography (chloroform / methanol / triethylamine).

The obtained product was dissolved in THF and a catalytic amount of conc. HCl was added and the reaction mixture was stirred at room temperature and controlled by TLC. After that the solvent was evaporated under vacuum and the hydroxamic acid product was purified by column chromatography (chloroform / methanol / formic acid). The yields were around 30-50%.

Other specific synthetic methods for some intermediates are provided in (**S1- supplementary**).

8.1.3. Characterization data of the final compounds

5a; *N*-[5-(hydroxycarbamoyl)-2-chlorophenyl]-biphenyl-4-carboxamide

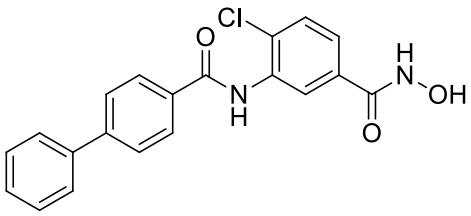

This compound was synthesized – as shown in scheme **1** – through the amide coupling between biphenyl-4-carboxylic acid **1a** and methyl 3-amino-4-chlorobenzoate **2a** using method B. The resulting ester was hydrolyzed using method F to afford *N*-[5-(hydroxycarbonyl)-2-chlorophenyl]-biphenyl-4-carboxamide **4a**.This acid was converted to the final compound using method G.
^{1}H NMR (400 MHz, DMSO-d_6) δ 11.33 (s, 1H), 10.21 (s, 1H), 9.12 (s, 1H), 8.11 – 8.06 (m, 2H), 8.01 (s, 1H), 7.87 – 7.82 (m, 2H), 7.78 – 7.73 (m, 2H), 7.68 – 7.62 (m, 2H), 7.54 – 7.47 (m, 2H), 7.45 – 7.39 (m, 1H).
HRMS m/z: 365.0699 $[M-H]^-$; calculated $C_{20}H_{14}N_2O_3Cl^-$ 365.0688
HPLC: rt 12.01 min (98.51%)

5b; *N*-[5-(hydroxycarbamoyl)-2-methylthiophenyl]-biphenyl-4-carboxamide

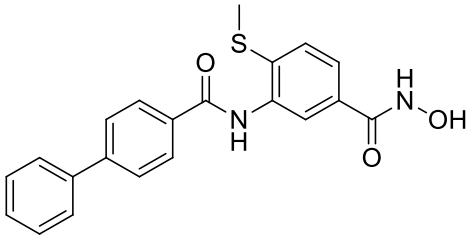

We have previously described the synthesis and characterization data of this compound [39]

5c; 3-(2-Chlor-4-phenylbenzamido)-*N*-hydroxy-4-methoxybenzamide

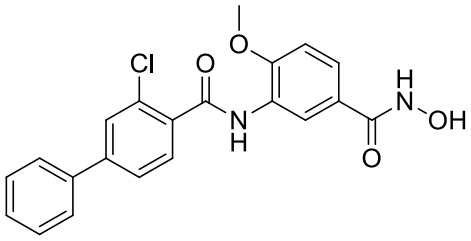

This compound was synthesized – as shown in scheme **1** – through the amide coupling between 2-chloro-4-phenylbenzoic acid **1b** and methyl 3-amino-4-methoxybenzoate **2c** using method B.

The resulting ester was hydrolyzed using method F to afford 3-(2-chlor-4-phenylbenzamido)-4-methoxybenzoic acid **4c**. This acid was converted to the final compound using method G.
^{1}H NMR (400 MHz, DMSO-d_6) δ 11.10 (s, 1H), 9.75 (s, 1H), 8.90 (s, 1H), 8.36 (s, 1H), 7.82 (s, 1H), 7.76-7.70 (m, 3H), 7.65 (d, J = 8.0 Hz, 1H), 7.58 (dd, J = 8.6, 2.1 Hz, 1H), 7.53-7.47 (m, 2H), 7.42 (t, J = 7.2 Hz, 1H), 7.12 (d, J = 8.5 Hz, 1H), 3.86 (s, 3H).
HRMS m/z: 397.0950 $[M+H]^+$; calculated $C_{21}H_{18}ClN_2O_4^+$ 397.0950
HPLC: rt 11.74 min (99.99 %)

5d; 3-(2-Chlor-4-phenylbenzamido)- 4-chloro-*N*-hydroxybenzamide

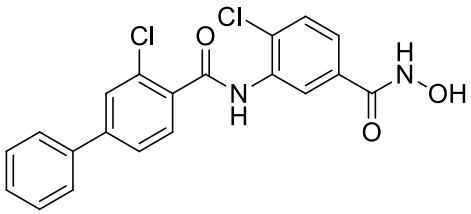

This compound was synthesized – as shown in scheme **1** – through the amide coupling between 2-chloro-4-phenylbenzoic acid **1b** and methyl 3-amino-4-chlorobenzoate **2a** using method B.
The resulting ester was hydrolyzed using method F to afford 3-(2-chlor-4-phenylbenzamido)-4-chlorobenzoic acid **4d**. This acid was converted to the final compound using method G.
^{1}H NMR (400 MHz, DMSO-d_6) δ 11.36 (s, 1H), 10.35 (s, 1H), 9.11 (s, 1H), 8.09 (s, 1H), 7.85 (s, 1H), 7.81 – 7.67 (m, 4H), 7.63 (s, 2H), 7.53-7.47 (m, 2H), 7.43 (t, J = 7.3 Hz, 1H).
HRMS m/z: 401.0461 $[M+H]^+$; calculated $C_{20}H_{15}Cl_2N_2O_3^+$ 401.0454
HPLC: rt 11.51 min (99.99%)
Yield: 65 mg; 0.16 mmol; 28%

5e; 3-[2-Chlor-4-(4-fluorphenyl)benzamido]-*N*-hydroxy-4-methoxybenzamide

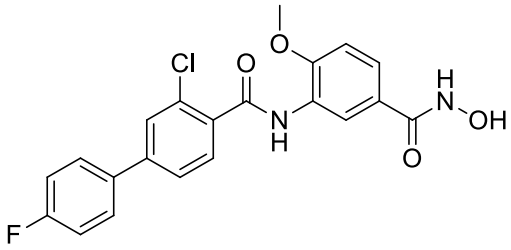

We have previously described the synthesis and characterization data of this compound [39]

5f; 3-[2-Chlor-4-(4-fluorphenyl-)benzamido]-4-chlor-*N*-hydroxybenzamide

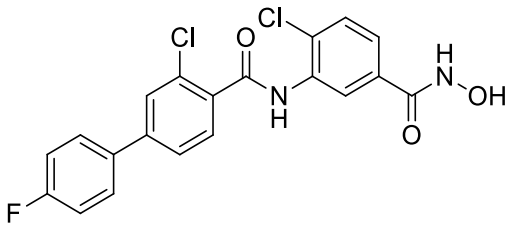

We have previously described the synthesis and characterization data of this compound [39]

5g; 4-Ethoxy-3-(4-methoxybenzamido)-*N*-hydroxybenzamide

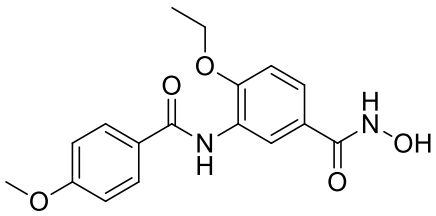

This compound was synthesized – as shown in scheme **1** – through the amide coupling between 4-methoxybenzoic acid **1d** and methyl 3-amino-4-ethoxybenzoate **2d** using method B. The resulting ester was hydrolyzed using method F to afford 3-(4-methoxybenzamido)-4-ethoxybenzoic acid **4g**. This acid was converted to the final compound using method G.
^{1}H NMR (400 MHz, DMSO-d_6) δ 11.11 (s, 1H), 9.29 (s, 1H), 8.97 (s, 1H), 8.18 (d, *J* = 2.2 Hz, 1H), 7.94 – 7.86 (m, 2H), 7.54 (dd, *J* = 8.6, 2.2 Hz, 1H), 7.08 (d, *J* = 8.7 Hz, 1H), 7.06 – 7.00 (m, 2H), 4.11 (q, *J* = 6.9 Hz, 2H), 3.80 (s, 3H), 1.38 – 1.27 (m, 3H).
HRMS m/z: 331.1285 $[M+H]^+$; calculated $C_{17}H_{19}N_2O_5^+$ 331.1289
HPLC: rt 12.23 min (99.81%)

5h; *N*-hydroxy-4-methoxy-3-(4-propoxybenzamido)benzamide

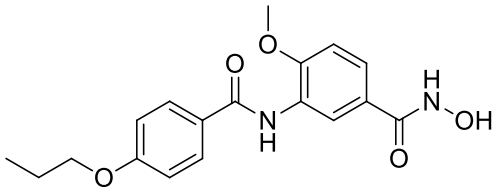

This compound was synthesized – as shown in scheme **1** – through the amide coupling between 4-propoxybenzoic acid **1e** and methyl 3-amino-4-methoxybenzoate **2c** using method B. The resulting ester was hydrolyzed using method F to afford 4-methoxy-3-(4-propoxybenzamido)benzoic acid **4h**. This acid was converted to the final compound using method G.
^{1}H NMR (400 MHz, DMSO-d_6) δ 11.07 (s, 1H), 9.34 (s, 1H), 8.88 (s, 1H), 8.16 (d, J = 2.1 Hz, 1H), 7.92 (d, J = 8.8 Hz, 2H), 7.58 (dd, J = 8.6, 2.2 Hz, 1H), 7.12 (d, J = 8.7 Hz, 1H), 7.03 (d, J = 8.9 Hz, 2H), 4.05 – 3.95 (m, 2H), 3.86 (s, 3H), 1.82 – 1.67 (m, 2H), 0.98 (t, J = 7.4 Hz, 3H).
HRMS m/z: 345.1446 $[M+H]^+$; calculated $C_{18}H_{21}N_2O_5^+$ 345.1445
HPLC: rt 10.57 min (99.99%)

5i; *N*-hydroxy-3-(4-isopropoxybenzamido)-4-methoxybenzamide

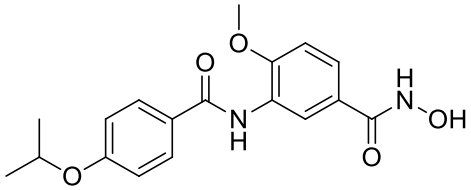

This compound was synthesized – as shown in scheme **1** – through the amide coupling between 4-isopropoxybenzoic acid **1f** and methyl 3-amino-4-methoxybenzoate **2c** using method B. The resulting ester was hydrolyzed using method F to afford 3-(4-isopropoxybenzamido)-4-methoxybenzoic acid **4i**. This acid was converted to the final compound using method G.
^{1}H NMR (400 MHz, DMSO-d_6) δ 11.07 (s, 1H), 9.32 (s, 1H), 8.88 (s, 1H), 8.17 (d, J = 2.2 Hz, 1H), 7.94 – 7.87 (m, 2H), 7.58 (dd, J = 8.6, 2.2 Hz, 1H), 7.11 (d, J = 8.7 Hz, 1H), 7.04 – 6.97 (m, 2H), 4.79 – 4.64 (m, 1H), 3.86 (s, 3H), 1.28 (d, *J* = 6.0 Hz, 6H).
HRMS m/z: 345.1445 $[M+H]^+$; calculated $C_{18}H_{21}N_2O_5^+$ 345.1445
HPLC: rt 10.12 min (99.99 %)

5j; 3-(2,4-Dimethoxybenzamido)-*N*-hydroxy-4-methoxybenzamide

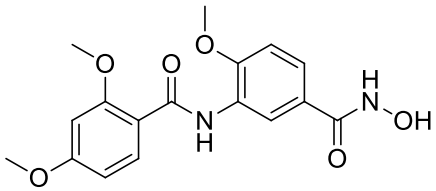

This compound was synthesized – as shown in scheme **1** – through the amide coupling between 2,4-dimethoxybenzoic acid **1g** and methyl 3-amino-4-methoxybenzoate **2c** using method B. The resulting ester was hydrolyzed using method F to afford 3-(2,4-dimethoxybenzamido)-4-methoxybenzamide **4j**. This acid was converted to the final compound using method G.
^{1}H NMR (400 MHz, DMSO-d_6) δ 11.04 (s, 1H), 10.53 (s, 1H), 8.90-8.84 (m, 2H), 8.04 (d, J = 8.7 Hz, 1H), 7.44 (dd, J = 8.5, 2.1 Hz, 1H), 7.11 (d, J = 8.6 Hz, 1H), 6.78 – 6.70 (m, 2H), 4.07 (s, 3H), 3.99 (s, 3H), 3.85 (s, 3H).
HRMS m/z: 347.1237 $[M+H]^+$; calculated $C_{17}H_{19}N_2O_6^+$ 347.1238
HPLC: rt 10.85 min (92.03%)

5k; 3-(2,4-Dichlorbenzamido)-4-ethoxy-*N*-hydroxybenzamide

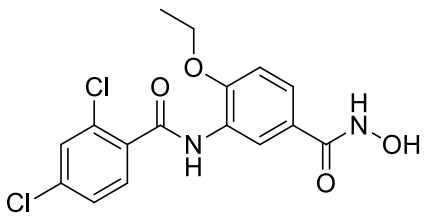

This compound was synthesized – as shown in scheme **1** – through the amide coupling between 2,4-dichlorobenzoic acid **1h** and methyl 3-amino-4-ethoxybenzoate **2d** using method B. The resulting ester was hydrolyzed using method F to afford 3-(2,4-dichlorobenzamido)-4-ethoxybenzoic acid **4k**. This acid was converted to the final compound using method G.
^{1}H NMR (400 MHz, DMSO-d_6) δ 11.10 (s, 1H), 9.74 (s, 1H), 8.93 (s, 1H), 8.25 (d, *J* = 1.3 Hz, 1H), 7.71 (d, *J* = 1.4 Hz, 1H), 7.63 – 7.49 (m, 3H), 7.09 (d, *J* = 8.6 Hz, 1H), 4.11 (q, *J* = 6.9 Hz, 2H), 1.32 (t, *J* = 6.9 Hz, 3H).
HRMS m/z: 391.0217 $[M+Na]^+$; calculated $C_{16}H_{14}N_2O_4Cl_2Na^+$ 391.0223
HPLC: rt 12.94 min (98.85%)

5l; 3-(4-Acetyl-2-propoxy-benzamido)-*N*-hydroxy-4-methylbenzamide

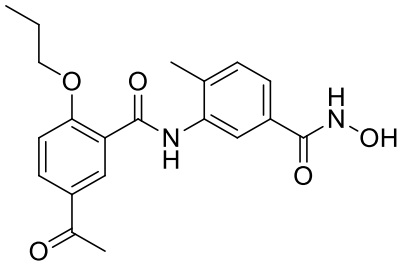

We have previously described the synthesis and characterization data of this compound [39]
5m; *N*-(5-(hydroxycarbamoyl)-2-methoxyphenyl)-1*H*-benzo[d]imidazole-2-carboxamide

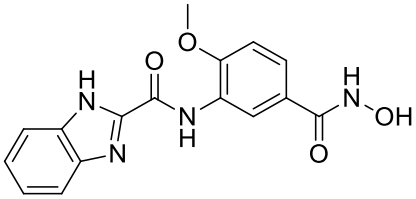

This compound was synthesized – as shown in scheme **1** – through the amide coupling between 1*H*-benzimidazole-2-carboxylic acid **1j** and methyl 3-amino-4-methoxybenzoate **2c** using method B. The resulting ester was hydrolyzed using method F to afford *N*-[5-(hydroxycarbonyl)-2-methoxyphenyl]-1*H*-benzo[d]imidazole-2-carboxamide **4m**. This acid was converted to the final compound using method G.
^{1}H NMR (500 MHz, DMSO-d_6) δ 13.55 (s, 1H), 11.13 (s, 1H), 9.91 (s, 1H), 8.92 (s, 1H), 8.72 (d, *J* = 1.7 Hz, 1H), 7.80 (d, *J* = 7.3 Hz, 1H), 7.60-7.52 (m, 2H), 7.39 – 7.27 (m, 2H), 7.19 (d, *J* = 8.1 Hz, 1H), 3.99 (s, 3H).
HRMS m/z: 327.1117 $[M+H]^+$; calculated $C_{16}H_{15}N_4O_4^+$ 327.1093
HPLC: rt 10.29 min (98.85 %)

5n; *N*-(5-(hydroxycarbamoyl)-2-methoxyphenyl)quinoline-8-carboxamide

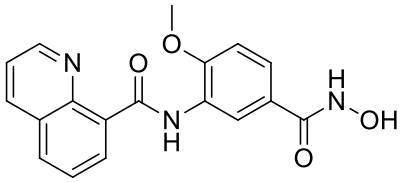

This compound was synthesized – as shown in scheme **1** – through the amide coupling between 8-quinolinecarboxylic acid **1k** and methyl 3-amino-4-methoxybenzoate **2c** using method B. The resulting ester was hydrolyzed using method F to afford *N*-(5-(hydroxycarbonyl)-2-methoxyphenyl)quinoline-8-carboxamide **4n**. This acid was converted to the final compound using method G.
^{1}H NMR (400 MHz, DMSO-d_6) δ 11.07 (s, 1H), 9.18 (dd, *J* = 4.2, 1.8 Hz, 1H), 9.03 (d, *J* = 2.1 Hz, 1H), 8.88 (s, 1H), 8.78 (dd, *J* = 7.4, 1.5 Hz, 1H), 8.65 (dd, *J* = 8.4, 1.8 Hz, 1H), 8.29 (dd, *J* = 8.1, 1.5 Hz, 1H), 7.86 – 7.82 (m, 1H), 7.76 (dd, *J* = 8.3, 4.3 Hz, 1H), 7.49 (dd, *J* = 8.5, 2.2 Hz, 1H), 7.16 (d, *J* = 8.6 Hz, 1H), 4.08 (s, 3H).
HRMS m/z: 338.1130 $[M+H]^+$; calculated $C_{18}H_{16}N_3O_4^+$ 338.1140
HPLC: rt 10.32 min (98.50%)

5o; *N*-[5-(hydroxycarbamoyl)-2-methoxyphenyl]-dibenzofuran-4-carboxamide

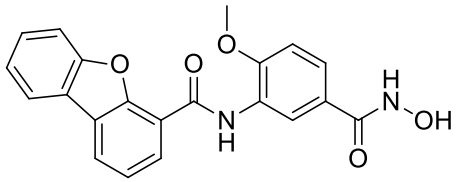

This compound was synthesized – as shown in scheme **1** – through the amide coupling between dibenzofuran-4-carboxylic acid **1l** and methyl 3-amino-4-methoxybenzoate **2c** using method B. The resulting ester was hydrolyzed using method F to afford *N*-[5-(hydroxycarbonyl)-2-methoxyphenyl]-dibenzofuran-4-carboxamide **4o**. This acid was converted to the final compound using method G.
^{1}H NMR (400 MHz, DMSO-d_6) δ 11.12 (s, 1H), 10.20 (s, 1H), 9.07-8.74 (m, 2H), 8.40 (d, *J* = 7.6 Hz, 1H), 8.24 (d, *J* = 7.8 Hz, 1H), 8.14 (d, *J* = 7.5 Hz, 1H), 7.83 (d, *J* = 8.1 Hz, 1H), 7.64 – 7.44 (m, 4H), 7.21 (d, *J* = 8.5 Hz, 1H), 4.10 (s, 3H).
HRMS m/z: 377.1132 $[M+H]^+$; calculated $C_{21}H_{17}N_2O_5^+$ 377.1137
HPLC: rt 9.90 min (96.10%)

5p; *N*-[5-(hydroxycarbamoyl)-2-methoxyphenyl]-9-(hydroxyimino)-9*H*-fluorene-1-carboxamide

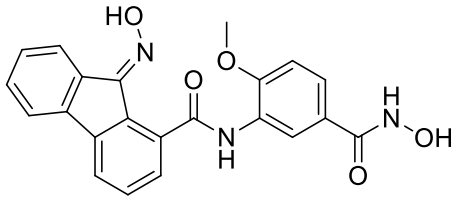

This compound was obtained as unexpected product instead of the originally planned compound *N*-[5-(hydroxycarbamoyl)-2-methoxyphenyl]-9-oxo-9*H*-fluorene-1-carboxamide.
The synthesis started – as shown in scheme **1** – through the amide coupling between 9-fluorenone-1-carboxylic acid **1m** and methyl 3-amino-4-methoxybenzoate **2c** using method B. The resulting ester was hydrolyzed using method F to afford 4-methoxy-3-(9-oxo-9*H*-fluorene-1-carboxamido)benzoic acid **4p**. When method G was applied to this acid, it yielded the titled compound.
^{1}H NMR (400 MHz, DMSO-d_6) δ 12.65 (s, 1H), 11.05 (s, 1H), 9.81 (s, 1H), 8.90 (s, 1H), 8.64 (s, 1H), 8.36 (d, *J* = 7.6 Hz, 1H), 8.04 – 7.87 (m, 2H), 7.55 – 7.42 (m, 4H), 7.40 (t, *J* = 7.5 Hz, 1H), 7.08 (d, *J* = 8.6 Hz, 1H), 3.82 (s, 3H).
HRMS m/z: 426.1053 $[M+Na]^+$; calculated $C_{22}H_{17}N_3O_5Na^+$: 426.1060
HPLC: rt 11.77 min (99.6 %)

8; 3-[*N*-(dibenzofuran-4-yl-methyl)amino]-*N*-hydroxy-4-methoxybenzamide

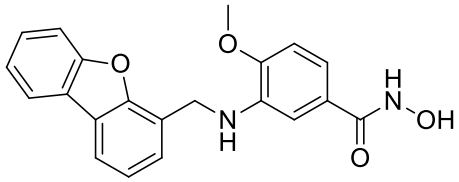

This compound was synthesized – as shown in scheme **2** – through reductive amination between dibenzofuran-4-carbaldehyde **6** and 3-amino-4-methoxybenzoic acid **2c-CA** using method D. The resulting 3-[*N*-(dibenzofuran-4-yl-methyl)amino]-4-methoxybenzoic acid **7** was converted to the final compound using method G.
^{1}H NMR (400 MHz, DMSO-d_6) δ 10.84 (s, 1H), 8.67 (s, 1H), 8.13 (d, J = 7.5 Hz, 1H), 8.00 (d, J = 7.2 Hz, 1H), 7.75 (d, J = 8.0 Hz, 1H), 7.53 (t, J = 7.7 Hz, 1H), 7.47 – 7.25 (m, 3H), 7.01 (dd, J = 8.2, 1.8 Hz, 1H), 6.96 (d, J = 1.9 Hz, 1H), 6.85 (d, J = 8.3 Hz, 1H), 5.71 (t, J = 6.2 Hz, 1H), 4.74 (d, J = 6.0 Hz, 2H), 3.85 (s, 3H).
HRMS m/z: 363.1332 $[M+H]^+$; calculated $C_{21}H_{19}N_2O_4^+$ 363.1344
HPLC: rt 8.87 min (91.77%)

13a; 3-(4-Chlorophenylcarbamoyl)-*N*-hydroxy-4-methoxybenzamide

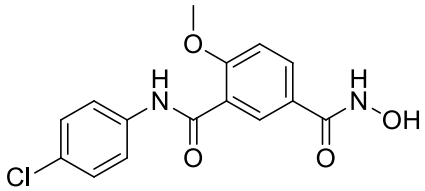

We have previously described the synthesis and characterization data of this compound [36]

13b; 4-Chloro-3-(4-chlorophenylcarbamoyl)-*N*-hydroxybenzamide

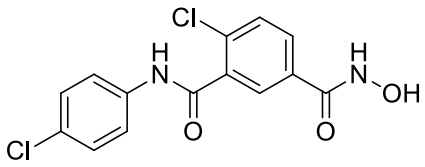

We have previously described the synthesis and characterization data of this compound [36]

13c; 3-(4-Chlorophenylcarbamoyl)-*N*-hydroxy-4-methylbenzamide

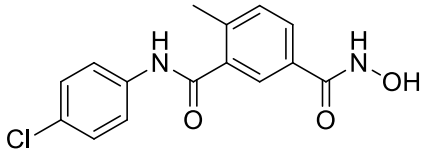

We have previously described the synthesis and characterization data of this compound [36]

13d; 3-(4-Acetyl-2-ethoxy-phenylcarbamoyl)-*N*-hydroxybenzamide

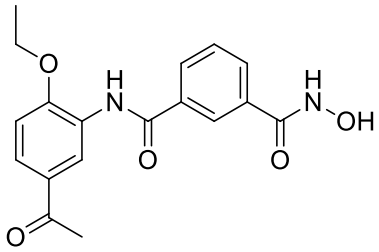

This compound was synthesized – as shown in scheme **3** – through the amide coupling between 3-(methoxycarbonyl)benzoic acid **10a** and 1-(3-amino-4-ethoxyphenyl)ethanone **9b** using method A. The resulting ester was hydrolyzed using method F to afford 3-[(5-acetyl-2-ethoxyphenyl)carbamoyl]benzoic acid **12d**. This acid was converted to the final compound using method G.
^{1}H NMR (400 MHz, DMSO-d_6) δ 11.32 (s, 1H), 9.64 (s, 1H), 9.12 (s, 1H), 8.36 – 8.30 (m, 2H), 8.09 – 8.03 (m, 1H), 7.95 – 7.90 (m, 1H), 7.83 (dd, *J* = 8.6, 2.2 Hz, 1H), 7.61 (t, *J* = 7.8 Hz, 1H), 7.19 (d, *J* = 8.7 Hz, 1H), 4.20 (q, J = 7.0 Hz, 2H), 2.52 (s, 3H), 1.36 (t, J = 7.0 Hz, 3H).
HRMS m/z: 343.1315 $[M+H]^+$; calculated $C_{18}H_{19}N_2O_5^+$: 343.1293
HPLC: rt 7.87 min (98.89 %)

13e; 3-(4-Acetyl-2-methoxy-phenylcarbamoyl)-*N*-hydroxy-4-methoxybenzamide

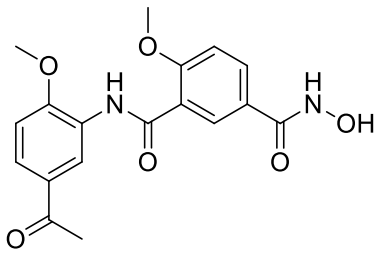

This compound was synthesized – as shown in scheme **3** – through the amide coupling between 2-methoxy-5-(methoxycarbonyl)benzoic acid **10b** and 1-(3-amino-4-methoxyphenyl)ethanone **9c** using method A. The resulting ester was hydrolyzed using method F to afford 3-[(5-acetyl-2-methoxyphenyl)carbamoyl]-4-methoxybenzoic acid **12e**. This acid was converted to the final compound using method G.
^{1}H NMR (400 MHz, DMSO-d_6) δ 11.27 (s, 1H), 10.59 (s, 1H), 9.18 – 8.88 (m, 2H), 8.59 – 8.47 (m, 1H), 7.96 (d, *J* = 8.7 Hz, 1H), 7.77 (d, *J* = 8.6 Hz, 1H), 7.35 (d, *J* = 8.6 Hz, 1H), 7.20 (d, *J* = 8.4 Hz, 1H), 4.12 (s, 3H), 4.04 (s, 3H), 2.53 (s, 3H).
HRMS m/z: 359.1231 $[M+H]^+$; calculated $C_{18}H_{19}N_2O_6^+$: 359.1243
HPLC: rt 10.74 min (99.72 %)

13f; 3-(4-Acetyl-2-ethoxy-phenylcarbamoyl)-*N*-hydroxy-4-methoxybenzamide

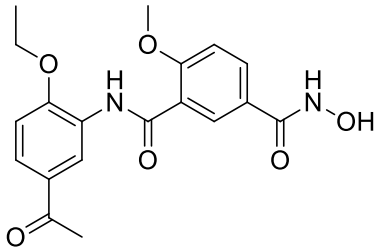

This compound was synthesized – as shown in scheme **3** – through the amide coupling between 2-methoxy-5-(methoxycarbonyl)benzoic acid **10b** and 1-(3-amino-4-ethoxyphenyl)ethanone **9b** using method A. The resulting ester was hydrolyzed using method F to afford 3-[(5-acetyl-2-ethoxyphenyl)carbamoyl]-4-methoxybenzoic acid **12f**. This acid was converted to the final compound using method G.
^{1}H NMR (400 MHz, DMSO-d_6) δ 11.27 (s, 1H), 10.45 (s, 1H), 9.10 (d, *J* = 2.1 Hz, 1H), 8.99 (s, 1H), 8.54 (d, *J* = 2.3 Hz, 1H), 7.97 (dd, *J* = 8.7, 2.4 Hz, 1H), 7.75 (dd, *J* = 8.6, 2.2 Hz, 1H), 7.36 (d, *J* = 8.8 Hz, 1H), 7.19 (d, *J* = 8.6 Hz, 1H), 4.27 (q, J = 7.0 Hz, 2H), 4.11 (s, 3H), 2.53 (s, 3H), 1.49 (t, *J* = 6.9 Hz, 3H).
HRMS m/z: 373.1384 $[M+H]^+$; calculated $C_{19}H_{21}N_2O_6^+$: 373.1399
HPLC: rt 10.57 min (99.97 %)

13g; 3-(4-Acetyl-2-methoxy-phenylcarbamoyl)-4-chloro-*N*-hydroxybenzamide

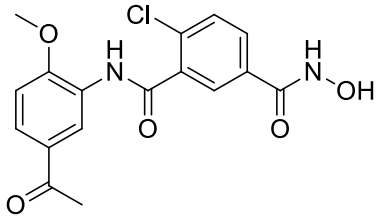

This compound was synthesized – as shown in scheme **3** – through the amide coupling between 2-chloro-5-(methoxycarbonyl)benzoic acid **10c** and 1-(3-amino-4-methoxyphenyl)ethanone **9c** using method A. The resulting ester was hydrolyzed using method F to afford 3-[(5-acetyl-2-

methoxyphenyl)carbamoyl]-4-chlorobenzoic acid **12g**. This acid was converted to the final compound using method G.
^{1}H NMR (400 MHz, DMSO-d_6) δ 11.37 (s, 1H), 9.94 (s, 1H), 9.15 (s, 1H), 8.51 (d, *J* = 1.8 Hz, 1H), 7.93 (d, *J* = 1.7 Hz, 1H), 7.88 – 7.78 (m, 2H), 7.63 (d, *J* = 8.4 Hz, 1H), 7.19 (d, *J* = 8.7 Hz, 1H), 3.90 (s, 3H), 2.53 (s, 3H).
HRMS m/z: 363.0734 $[M+H]^+$; calculated $C_{17}H_{16}ClN_2O_5^+$: 363.0747
HPLC: rt 8.33 min (99.55 %)

13h; 3-(4-Acetyl-2-ethoxy-phenylcarbamoyl)-4-chloro-*N*-hydroxybenzamide

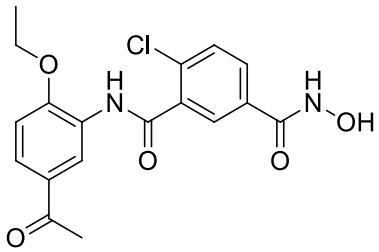

We have previously described the synthesis and characterization data of this compound [39]

13i; 3-(4-Acetyl-2-methoxy-phenylcarbamoyl)-*N*-hydroxy-4-methylbenzamide

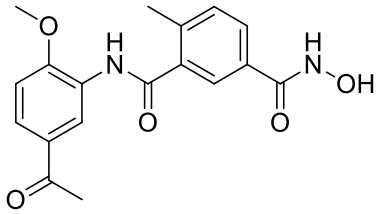

This compound was synthesized – as shown in scheme **3** – through the amide coupling between 5-(methoxycarbonyl)-2-methylbenzoic acid **10d** and 1-(3-amino-4-methoxyphenyl)ethanone **9c** using method A. The resulting ester was hydrolyzed using method F to afford 3-[(5-acetyl-2-methoxyphenyl)carbamoyl]-4-methylbenzoic acid **12i**. This acid was converted to the final compound using method G.
^{1}H NMR (400 MHz, DMSO-d_6) δ 11.22 (s, 1H), 9.59 (s, 1H), 9.03 (s, 1H), 8.41 (s, 1H), 7.90 – 7.80 (m, 2H), 7.75 (dd, *J* = 7.9, 1.5 Hz, 1H), 7.36 (d, *J* = 8.0 Hz, 1H), 7.19 (d, *J* = 8.6 Hz, 1H), 3.90 (s, 3H), 2.53 (s, 3H), 2.43 (s, 3H).
HRMS m/z: 343.1281 $[M+H]^+$; calculated $C_{18}H_{19}N_2O_5^+$: 343.1293
HPLC: rt 8.03 min (99.88 %)

13j; 3-(4-Acetyl-2-ethoxy-phenylcarbamoyl)-*N*-hydroxy-4-methylbenzamide

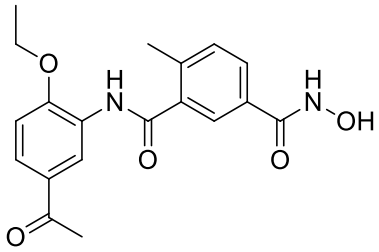

We have previously described the synthesis and characterization data of this compound [39]

13k; 3-(3-Chlorophenylcarbamoyl)-*N*-hydroxy-4-methoxybenzamide

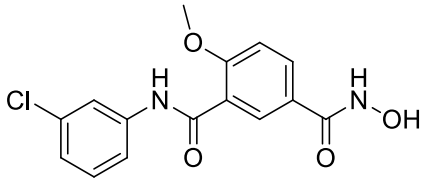

This compound was synthesized – as shown in scheme **3** – through the amide coupling between 2-methoxy-5-(methoxycarbonyl)benzoic acid **10b** and 3-chloroaniline **9d** using method A. The resulting ester was hydrolyzed using method F to afford 3-[(3-chlorophenyl)carbamoyl]-4-methoxybenzoic acid **12k**. This acid was converted to the final compound using method G.
^{1}H NMR (400 MHz, DMSO-d_6) δ 11.18 (s, 1H), 10.32 (s, 1H), 8.96 (s, 1H), 7.99 (d, *J* = 2.3 Hz, 1H), 7.93 – 7.87 (m, 2H), 7.61 (d, *J* = 9.1 Hz, 1H), 7.36 (t, *J* = 8.1 Hz, 1H), 7.23 (d, *J* = 8.8 Hz, 1H), 7.16-7.12 (m, 1H), 3.91 (s, 3H).
HRMS m/z: 321.0642 $[M+H]^+$; calculated $C_{15}H_{14}ClN_2O_4^+$: 321.0642
HPLC: rt 11.14 min (98.18 %)

13l; *N*-Hydroxy-4-methoxy-3-(4-methoxyphenylcarbamoyl)benzamide

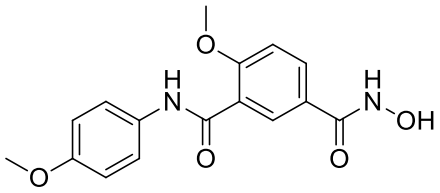

This compound was synthesized – as shown in scheme **3** – through the amide coupling between 2-methoxy-5-(methoxycarbonyl)benzoic acid **10b** and 4-methoxyaniline **9e** using method A. The resulting ester was hydrolyzed using method F to afford 4-methoxy-3-[(4-methoxyphenyl)carbamoyl]benzoic acid **12l**. This acid was converted to the final compound using method G.
^{1}H NMR (400 MHz, DMSO-d_6) δ 11.17 (s, 1H), 9.99 (s, 1H), 8.94 (s, 1H), 8.01 (d, *J* = 2.3 Hz, 1H), 7.88 (dd, *J* = 8.7, 2.4 Hz, 1H), 7.65 – 7.59 (m, 2H), 7.21 (d, *J* = 8.8 Hz, 1H), 6.93 – 6.87 (m, 2H), 3.91 (s, 3H), 3.73 (s, 3H).
HRMS m/z: 317.1128 $[M+H]^+$; calculated $C_{16}H_{17}N_2O_5^+$: 317.1137

HPLC: rt 9.62 min (97.27 %)

13m; 3-(2,4-Dichlorophenylcarbamoyl)-*N*-hydroxy-4-methoxybenzamide

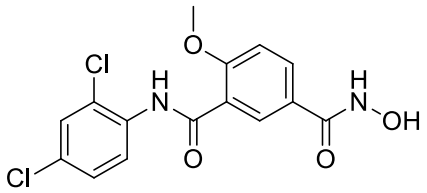

This compound was synthesized – as shown in scheme **3** – through the amide coupling between 2-methoxy-5-(methoxycarbonyl)benzoic acid **10b** and 2,4-dichloroaniline **9f** using method A. The resulting ester was hydrolyzed using method F to afford 3-[(2,4-dichlorophenyl)carbamoyl]-4-methoxybenzoic acid **12m**. This acid was converted to the final compound using method G.
^{1}H NMR (400 MHz, DMSO-d_6) δ 11.29 (s, 1H), 10.57 (s, 1H), 9.01 (s, 1H), 8.53 (d, *J* = 1.9 Hz, 1H), 8.47 (d, *J* = 2.1 Hz, 1H), 8.01 – 7.95 (m, 1H), 7.60 (d, *J* = 8.6 Hz, 1H), 7.36 (d, *J* = 8.6 Hz, 1H), 7.25 (dd, *J* = 8.6, 2.4 Hz, 1H), 4.11 (s, 3H).
HRMS m/z: 355.0261 $[M+H]^+$; calculated $C_{15}H_{13}Cl_2N_2O_4^+$: 355.0252
HPLC: rt 11.51 min (99.67 %)

13n; 3-(Benzo[b]thiophen-5-carbamoyl)-*N*-hydroxy-4-methoxybenzamide

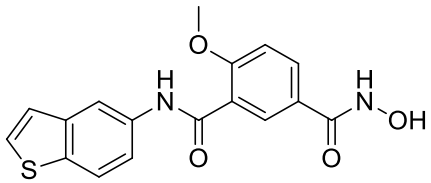

This compound was synthesized – as shown in scheme **3** – through the amide coupling between 2-methoxy-5-(methoxycarbonyl)benzoic acid **10b** and benzo[b]thiophen-5-amine **9g** using method A. The resulting ester was hydrolyzed using method F to afford 3-(benzo[b]thiophen-5-ylcarbamoyl)-4-methoxybenzoic acid **12n**. This acid was converted to the final compound using method G.
^{1}H NMR (400 MHz, DMSO-d_6) δ 11.19 (s, 1H), 10.26 (s, 1H), 8.96 (s, 1H), 8.39 (d, *J* = 1.9 Hz, 1H), 8.04 (d, *J* = 2.3 Hz, 1H), 7.95 – 7.88 (m, 2H), 7.75 (d, *J* = 5.4 Hz, 1H), 7.59 (dd, *J* = 8.7, 1.9 Hz, 1H), 7.44 (d, *J* = 5.4 Hz, 1H), 7.24 (d, *J* = 8.8 Hz, 1H), 3.93 (s, 3H).
HRMS m/z: 343.0747 $[M+H]^+$; calculated $C_{17}H_{15}N_2O_4S^+$: 343.0752
HPLC: rt 11.81 min (100 %)

19a; 3-[3-[Benzyloxy]benzamido]-*N*-hydroxy-4-methoxybenzamide

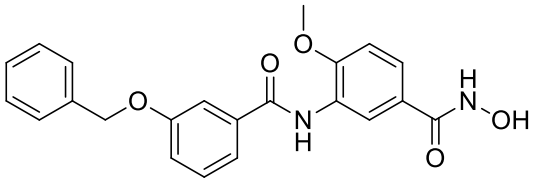

This compound was synthesized – as shown in scheme **4** – through Williamson ether synthesis between benzyl bromide **14a** and methyl 3-hydroxybenzoate **15** using method E. The resulting ester was hydrolyzed using method F to afford 3-(benzyloxy)benzoic acid **16a**, which was coupled with methyl 3-amino-4-methoxybenzoate **2c** using method B. The resulted ester was again hydrolyzed using method F to afford 3-[3-(benzyloxy)benzamido]-4-methoxybenzoic acid **18a**, which was then converted to the final compound using method G.
^{1}H NMR (400 MHz, DMSO-d_6) δ 11.09 (s, 1H), 9.51 (s, 1H), 8.89 (s, 1H), 8.12 (d, *J* = 2.2 Hz, 1H), 7.63 – 7.56 (m, 2H), 7.54 (d, *J* = 7.8 Hz, 1H), 7.48 – 7.30 (m, 6H), 7.22 (dd, *J* = 8.1, 2.0 Hz, 1H), 7.13 (d, *J* = 8.7 Hz, 1H), 5.18 (s, 2H), 3.86 (s, 3H).
HRMS m/z: 415.1285 $[M+Na]^+$; calculated $C_{22}H_{20}N_2O_5Na^+$ 415.1269
HPLC: rt 11.06 min (98.69 %)

19b; 3-[3-[Benzyloxy]benzamido]-*N*-hydroxy-4-methylbenzamide

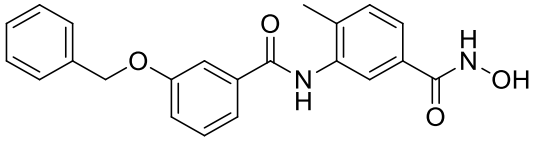

This compound was synthesized – as shown in scheme **4** – through Williamson ether synthesis between benzyl bromide **14a** and methyl 3-hydroxybenzoate **15** using method E. The resulting ester was hydrolyzed using method F to afford 3-(benzyloxy)benzoic acid **16a**, which was coupled with methyl 3-amino-4-methylbenzoate **2e** using method B. The resulted ester was again hydrolyzed using method F to afford 3-[3-(benzyloxy)benzamido]-4-methylbenzoic acid **18b**, which was then converted to the final compound using method G.
^{1}H NMR (400 MHz, DMSO-d_6) δ 11.17 (s, 1H), 9.95 (s, 1H), 8.97 (s, 1H), 7.74 (d, *J* = 1.6 Hz, 1H), 7.62 – 7.60 (m, 1H), 7.58 – 7.53 (m, 2H), 7.49 – 7.36 (m, 5H), 7.35 – 7.30 (m, 2H), 7.25 – 7.21 (m, 1H), 5.18 (s, 2H), 2.24 (s, 3H).
HRMS m/z: 399.1357 $[M+Na]^+$; calculated $C_{22}H_{20}N_2O_4Na^+$ 399.1320
HPLC: rt 11.03 min (99.22 %)

19c; 3-[3-[2,6-Dichlorbenzyloxy]benzamido]-*N*-hydroxy-4-methylbenzamide

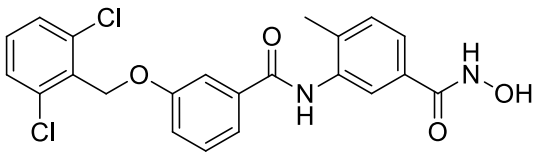

This compound was synthesized – as shown in scheme **4** – through Williamson ether synthesis between 2,6-dichlorobenzyl bromide **14b** and methyl 3-hydroxybenzoate **15** using method E. The resulting ester was hydrolyzed using method F to afford 3-(2,6-dichlorobenzyloxy)benzoic acid **16b**, which was coupled with methyl 3-amino-4-methylbenzoate **2e** using method B. The resulted ester was again hydrolyzed using method F to afford 3-[3-(2,6-dichlorobenzyloxy)benzamido]-4-methylbenzoic acid **18c**, which was then converted to the final compound using method G.
^{1}H NMR (400 MHz, DMSO-d_6) δ 11.19 (s, 1H), 10.00 (s, 1H), 8.99 (s, 1H), 7.79 – 7.26 (m, 10H), 5.32 (s, 2H), 2.26 (s, 3H).
HRMS m/z: 467.0533 $[M+Na]^+$; calculated $C_{22}H_{18}N_2O_4Cl_2Na^+$: 467.0536
HPLC: rt 12.05 min (98.5 %)

24 ; *N*-(5-(hydroxycarbamoyl)-2-methoxyphenyl)-2-methyl-2,3,4,5-tetrahydro-1*H*-pyrido[4,3-*b*]indole-8-carboxamide hydrochloride

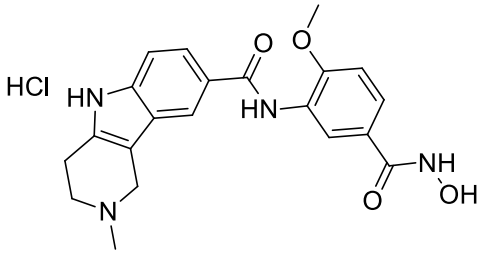

This compound was synthesized – as shown in scheme **5** – through the amide coupling between 2-methyl-2,3,4,5-tetrahydro-1*H*-pyrido[4,3-b]indole-8-carboxylic acid **23** and 3-amino-4-methoxy-*N*-(tetrahydro-2*H*-pyran-2-yloxy)benzamide **20** using method C. The THP protected product was then deprotected with HCl - as described in method G. The product was directly purified using preparative HPLC.
^{1}H NMR (400 MHz, DMSO-D_6) δ 11.58 (s, 1H), 11.09 (s, 1H), 10.94 (s, 1H), 10.01 (s, 1H), 9.30 (s, 1H), 8.25 (d, J = 2.1 Hz, 1H), 8.12 (s, 1H), 7.74 (dd, J = 8.6, 1.5 Hz, 1H), 7.58 (dd, J = 8.6, 2.1 Hz, 1H), 7.44 (d, J = 8.5 Hz, 1H), 7.13 (d, J = 8.7 Hz, 1H), 3.88 (s, 2H), 3.32 (s, 3H), 3.15 – 2.99 (m, 4H), 2.96 (s, 3H).
HRMS m/z: 395.1708 $[M+H]^+$; calculated $C_{21}H_{23}N_4O_4^+$ 395.1719
HPLC: rt 6.97 min (97.62 %)

8.2. In vitro HDAC inhibitory activity

The *in vitro* testing on recombinant HDACs were performed as previously described [40].

Recombinant human HDAC1 and -6 were purchased from BPS Biosciences. The enzyme inhibition was determined by using a reported homogenous fluorescence assay [41]. The enzymes were incubated for 90 min at 37 °C, with the fluorogenic substrate ZMAL (Z-(Ac)Lys-AMC) in a concentration of 10.5 μM and increasing concentrations of inhibitors with subsequent

addition of 60 µL of buffer containing trypsin (1 mg/mL) and TSA (2.75 µM) and further incubation for 20 minutes at 37°C. Fluorescence intensity was measured at an excitation wavelength of 390 nm and an emission wavelength of 460 nm in a microtiter plate reader (BMG Polarstar).

Recombinant Sm- and hHDAC8 was produced by Romier *et al.* in Strasbourg [32, 35]. The HDAC8 activity assays were performed according to the commercial HDAC8 Fluorometric Drug Discovery Kit [Fluor de Lys(R)-HDAC8, BML-KI178] corresponding to the manufacturer´s instructions as described earlier [32]. As substrate a tetrapeptide connected to aminomethylcoumarin (AMC) H_2N-Arg-His-Lys(Ac)-Lys(Ac)-AMC was synthesized as previously described [40]. The enzyme was incubated for 90 min at 37 °C, with a substrate concentration of 50 µM and increasing concentrations of inhibitors. The stop-solution containing inhibitor, to stop the hHDAC8 activity, and Trypsin, to release the AMC, was added. The solution was incubated for 20 min at 37 °C to develop the assay. Fluorescence intensity was measured at an excitation wavelength of 355 nm and an emission wavelength of 460 nm in a microtiter plate reader (BMG Polarstar).

8.3. Cytotoxicity

To determine the cytotoxicity of the developed compounds, a human epithelial kidney cell line (HEK293) was used. HEK293 cells (DSMZ Braunschweig, ACC305) were incubated at 37°C in a humidified incubator with 5% CO_2 in Dulbecco's Modified Eagle Medium (DMEM) supplemented with 10 % fetal calf serum and 5 mM glutamine. Cells were seeded out at 1.5 x 10^3 cells per well in a 96-well cell culture plate (TPP, Switzerland). The compounds to be tested were added immediately to the medium at 50 µM. After 24 h, AlamarBlue reagent (Invitrogen, CA) was added according to the manufacturer's instructions and incubated again for 21 h before samples were analyzed. Detection of viable cells, which convert the resazurine reagent into the highly fluorescent resorufin, was performed by using a FLUOstarOPTIMA microplate reader (BMG Labtec) with the following filter set: Ex 530 nm / Em 590 nm. Measurements were performed in triplicate and data are means with standard deviation < 14%. As a positive control daunorubicin was used and an IC_{50} value of 12.55 ± 0.07 µM was measured.

8.4. Phenotypic screening

The effects of novel inhibitors targeting SmHDAC8 on the viability of *S. mansoni* schistosomula was carried out as previously described [34]. Briefly, newly transformed schistosomula (NTS) were obtained in vitro by mechanical transformation of *S. mansoni* cercariae as previously described [42]. An NTS suspension was prepared at a concentration of 100 NTS per 100 µL using Medium 199 (Invitrogen) supplemented with 10% fetal calf serum (Gibco), penicillin (50 U.mL-1), streptomycin (50 µg.mL-1) and rifampicin (60 µg.mL-1). Schistosomula were kept in culture 3 hours at 37°C and 5% CO_2 prior to use in screening. Stock solutions of 20 mM in DMSO were used for each inhibitor. Mid-dilutions were performed in 100% DMSO and 1 µl added to 100 µl/well of M199 medium in black 96 well plates (Nunc, UK) with supplemented

Medium 199 and 100 µl of prepared NTS suspension (100 NTS/well). Live and dead schistosomula (treated with 70% ethanol) were used as positive and negative controls. Experiments were carried out in triplicate wells in two biological replicates and the compounds were tested at final concentrations of 10 and 20 µM. After 48 hours of drug exposure, 20 µL of Alamar Blue solution (AbdSerotec) were added in each well. Finally, after a further 24 hours of exposure, the fluorescence intensity of the red fluorescent resorufin product was measured at an excitation wavelength of 530 nm and an emission wavelength of 590 nm in an Infinite M200 Pro microplate reader (TECAN). Background fluorescence of the drug containing medium was determined for each drug dilution using wells containing only DMSO as control. The EC_{50} concentration for compound **5o** was measured using the same assay with different concentrations of the compound.

8.5. Crystallization and X-ray data collection

Diffraction-quality crystals of native smHDAC8 enzyme were obtained at 17°C after three to four days by mixing equal volumes of smHDAC8 (2.5 mg/ml) with a reservoir solution composed of 21% PEG 3350 (Fluka) and 0.2 M Na+/K+ L-tartrate, and crystallized using the hanging-drop vapor diffusion technique. After 3 days, grown crystals were soaked in mother liquor supplemented with the inhibitor **5o** (10 mM final concentration of the inhibitor) for 20 hours. Crystals used for X-ray data collection were briefly transferred in reservoir solution supplemented with 22% glycerol and flash-frozen in liquid nitrogen. Crystallographic data obtained in this project were collected at 100 K on ESRF beamline ID23. Atomic coordinates and structure factors of the smHDAC8-5o complex were deposited in the Protein Data Bank under the PDB ID code 7P3S.

8.6. Molecular modelling studies

The available X-ray structure of smHDAC8 with compound **X** (TH65; PDB ID: 6HTH, chain A), hHDAC8 (PDB ID 2V5X), hDAC6 (PDB ID 5EDU) and hHDAC1 (PDB ID 4BKX) were downloaded from the Protein Data Bank (PDB¸; www.rcsb.org) [43]. Protein preparation was done using the protein preparation wizard implemented in Schrödinger version 2019.1 by adding hydrogen atoms, assigning protonation states and minimizing the protein. Ligands structures were generated in MOE [Molecular Operating Environment (MOE), 2020.01; Chemical Computing Group Inc., 1010 Sherbooke St. West, Suite #910, Montreal, QC, Canada, H3A 2R7, 2018] in the hydroxamte form. The ligands were subsequently prepared for docking using the LigPrep tool as implemented in Schrödinger's software (version 2019.1) and energy minimized using the OPLS3e force field. 25 conformers of all ligands were subsequently generated with ConfGen. Docking of the generated conformers into the prepared protein structures was performed using the program Glide (Schrödinger-release 2019.1) in the Standard Precision mode.

8.7. PAINS filter

All the herein described compounds were filtered for pan-assay interference compounds (PAINS) [44]. For this purpose, PAINS1, PAINS2 and PAINS3 filters, as implemented in Schrödinger's Canvas program, were employed. None of the compounds was flagged as a PAIN.

Author contribution

E.G. synthesized part of the compounds and wrote the paper. T.H., A.T., S.D. synthesized part of the compounds. P.Z. carried out the in vitro testing on HDAC8. K.S. carried out the in vitro testing on HDAC1 and 6. J.L. and R.J.P. performed antiparasitic studies and carried out data analysis. F.E. carried out the cellular testing on HEK293 cells. C.V.S. and D.R. did the docking calculations and wrote the manuscript. T.B.S. and C.R. solved the smHDAC8-inhibitor crystal structures. W.S., M.S. and M.J. designed experiments, analyzed data and wrote the paper. All authors have given approval to the final version of the manuscript

Acknowledgment

E.G. appreciated the support of DAAD Egypt by GERLS scholarship. This research was funded by the European Regional Development Fund of the European Commission. CR is supported by institutional funds from the Centre National de la Recherche Scientifique (CNRS), the Institut National de la Santé et de la Recherche Médicale (Inserm) and the Université de Strasbourg.

References

1. *Weekly Epidemiological Record," Schistosomiasis and soiltransmitted helminthiases: number of people treated in 2015"*. 2016 accessed 14.02.2020]; Available from: https://www.who.int/schistosomiasis/resources/who_wer914950/en/.
2. Rollinson, D., et al., *Time to set the agenda for schistosomiasis elimination.* Acta Trop, 2013. **128**(2): p. 423-40.
3. Doenhoff, M.J., et al., *Resistance of Schistosoma mansoni to praziquantel: is there a problem?* Trans R Soc Trop Med Hyg, 2002. **96**(5): p. 465-9.
4. Doenhoff, M.J., D. Cioli, and J. Utzinger, *Praziquantel: mechanisms of action, resistance and new derivatives for schistosomiasis.* Curr Opin Infect Dis, 2008. **21**(6): p. 659-67.
5. Marek, M., et al., *Drugging the schistosome zinc-dependent HDACs: current progress and future perspectives.* Future Med Chem, 2015. **7**(6): p. 783-800.
6. Mader, P., et al., *Chemotherapy for Fighting Schistosomiasis: Past, Present and Future.* ChemMedChem, 2018. **13**(22): p. 2374-2389.
7. Cabezas-Cruz, A., et al., *Epigenetic control of gene function in schistosomes: a source of therapeutic targets?* Front Genet, 2014. **5**(317): p. 317.
8. Pierce, R.J., et al., *Targeting schistosome histone modifying enzymes for drug development.* Curr Pharm Des, 2012. **18**(24): p. 3567-78.
9. Dissous, C. and C.G. Grevelding, *Piggy-backing the concept of cancer drugs for schistosomiasis treatment: a tangible perspective?* Trends Parasitol, 2011. **27**(2): p. 59-66.
10. Pierce, R.J., et al., *Chromatin regulation in schistosomes and histone modifying enzymes as drug targets.* Mem Inst Oswaldo Cruz, 2011. **106**(7): p. 794-801.

11. Suraweera, A., K.J. O'Byrne, and D.J. Richard, *Combination Therapy With Histone Deacetylase Inhibitors (HDACi) for the Treatment of Cancer: Achieving the Full Therapeutic Potential of HDACi.* Front Oncol, 2018. **8**: p. 92.
12. Khan, S.N. and A.U. Khan, *Role of histone acetylation in cell physiology and diseases: An update.* Clin Chim Acta, 2010. **411**(19-20): p. 1401-11.
13. Fan, J., et al., *Metabolic regulation of histone post-translational modifications.* ACS Chem Biol, 2015. **10**(1): p. 95-108.
14. Andrews, K.T., A. Haque, and M.K. Jones, *HDAC inhibitors in parasitic diseases.* Immunol Cell Biol, 2012. **90**(1): p. 66-77.
15. Hailu, G.S., et al., *Lysine Deacetylase Inhibitors in Parasites: Past, Present, and Future Perspectives.* J Med Chem, 2017. **60**(12): p. 4780-4804.
16. Bertrand, P., *Inside HDAC with HDAC inhibitors.* Eur J Med Chem, 2010. **45**(6): p. 2095-116.
17. Zhang, L., et al., *Zinc binding groups for histone deacetylase inhibitors.* J Enzyme Inhib Med Chem, 2018. **33**(1): p. 714-721.
18. Scholte, L.L.S., et al., *Evolutionary relationships among protein lysine deacetylases of parasites causing neglected diseases.* Infect Genet Evol, 2017. **53**: p. 175-188.
19. Lancelot, J., et al., *Schistosoma mansoni Sirtuins: characterization and potential as chemotherapeutic targets.* PLoS Negl Trop Dis, 2013. **7**(9): p. e2428.
20. Monaldi, D., et al., *Structure-Reactivity Relationships on Substrates and Inhibitors of the Lysine Deacylase Sirtuin 2 from Schistosoma mansoni (SmSirt2).* J Med Chem, 2019. **62**(19): p. 8733-8759.
21. Lancelot, J., et al., *Schistosome sirtuins as drug targets.* Future Med Chem, 2015. **7**(6): p. 765-82.
22. Dubois, F., et al., *Histone deacetylase inhibitors induce apoptosis, histone hyperacetylation and up-regulation of gene transcription in Schistosoma mansoni.* Mol Biochem Parasitol, 2009. **168**(1): p. 7-15.
23. Azzi, A., C. Cosseau, and C. Grunau, *Schistosoma mansoni: developmental arrest of miracidia treated with histone deacetylase inhibitors.* Exp Parasitol, 2009. **121**(3): p. 288-91.
24. Oger, F., et al., *The class I histone deacetylases of the platyhelminth parasite Schistosoma mansoni.* Biochem Biophys Res Commun, 2008. **377**(4): p. 1079-84.
25. Stenzel, K., et al., *Isophthalic Acid-Based HDAC Inhibitors as Potent Inhibitors of HDAC8 from Schistosoma mansoni.* Arch Pharm (Weinheim), 2017. **350**(8): p. 1700096.
26. Guidi, A., et al., *Identification of novel multi-stage histone deacetylase (HDAC) inhibitors that impair Schistosoma mansoni viability and egg production.* Parasit Vectors, 2018. **11**(1): p. 668.
27. Kalinin, D.V., et al., *Structure-Based Design, Synthesis, and Biological Evaluation of Triazole-Based smHDAC8 Inhibitors.* ChemMedChem, 2020. **15**(7): p. 571-584.
28. Saccoccia, F., et al., *Screening and Phenotypical Characterization of Schistosoma mansoni Histone Deacetylase 8 (SmHDAC8) Inhibitors as Multistage Antischistosomal Agents.* ACS Infect Dis, 2020. **6**(1): p. 100-113.
29. Fioravanti, R., et al., *Targeting histone acetylation/deacetylation in parasites: an update (2017-2020).* Curr Opin Chem Biol, 2020. **57**: p. 65-74.
30. Kannan, S., et al., *Discovery of inhibitors of Schistosoma mansoni HDAC8 by combining homology modeling, virtual screening, and in vitro validation.* J Chem Inf Model, 2014. **54**(10): p. 3005-19.
31. Simoben, C.V., et al., *A Novel Class of Schistosoma mansoni Histone Deacetylase 8 (HDAC8) Inhibitors Identified by Structure-Based Virtual Screening and In Vitro Testing.* Molecules, 2018. **23**(3): p. 566.
32. Marek, M., et al., *Structural basis for the inhibition of histone deacetylase 8 (HDAC8), a key epigenetic player in the blood fluke Schistosoma mansoni.* PLoS Pathog, 2013. **9**(9): p. e1003645.

33. Bayer, T., et al., *Synthesis, Crystallization Studies, and in vitro Characterization of Cinnamic Acid Derivatives as SmHDAC8 Inhibitors for the Treatment of Schistosomiasis.* ChemMedChem, 2018. **13**(15): p. 1517-1529.
34. Heimburg, T., et al., *Structure-Based Design and Synthesis of Novel Inhibitors Targeting HDAC8 from Schistosoma mansoni for the Treatment of Schistosomiasis.* J Med Chem, 2016. **59**(6): p. 2423-35.
35. Marek, M., et al., *Characterization of Histone Deacetylase 8 (HDAC8) Selective Inhibition Reveals Specific Active Site Structural and Functional Determinants.* J Med Chem, 2018. **61**(22): p. 10000-10016.
36. Heimburg, T., et al., *Structure-Based Design and Biological Characterization of Selective Histone Deacetylase 8 (HDAC8) Inhibitors with Anti-Neuroblastoma Activity.* J Med Chem, 2017. **60**(24): p. 10188-10204.
37. Simoben, C.V., et al., *Binding Free Energy (BFE) Calculations and Quantitative Structure–Activity Relationship (QSAR) Analysis of Schistosoma mansoni Histone Deacetylase 8 (smHDAC8) Inhibitors.* Molecules, 2021. **26**(9): p. 2584.
38. Suzuki, T., et al., *Rapid discovery of highly potent and selective inhibitors of histone deacetylase 8 using click chemistry to generate candidate libraries.* J Med Chem, 2012. **55**(22): p. 9562-75.
39. Vaca, H.R., et al., *The potential for histone deacetylase (HDAC) inhibitors as cestocidal drugs.* PLOS Neglected Tropical Diseases, 2021. **15**(3): p. e0009226.
40. Ghazy, E., et al., *Design, synthesis, and biological evaluation of dual targeting inhibitors of histone deacetylase 6/8 and bromodomain BRPF1.* Eur J Med Chem, 2020. **200**: p. 112338.
41. Stolfa, D.A., et al., *Design, synthesis, and biological evaluation of 2-aminobenzanilide derivatives as potent and selective HDAC inhibitors.* ChemMedChem, 2012. **7**(7): p. 1256-66.
42. Ramalho-Pinto, F.J., et al., *Schistosoma mansoni: Defined system for stepwise transformation of cercaria to schistosomule in vitro.* Experimental Parasitology, 1974. **36**(3): p. 360-372.
43. Berman, H.M., et al., *The Protein Data Bank.* Nucleic acids research, 2000. **28**(1): p. 235-242.
44. Baell, J.B. and G.A. Holloway, *New substructure filters for removal of pan assay interference compounds (PAINS) from screening libraries and for their exclusion in bioassays.* J Med Chem, 2010. **53**(7): p. 2719-40.